Ecohydrology & Hydrobiology xxx (xxxx) xxx

Contents lists available at ScienceDirect

Ecohydrology & Hydrobiology

journal homepage: www.elsevier.com/locate/ecohyd

Original Research Article

Role of transpiration in modulating ecosystem services in secondary tropical montane forests of Eastern Himalaya in India

Manish Kumar [a,b,c,*], Yangchenla Bhutia [b,c,d], Girish R Varma [e], Gladwin Joseph [b,c,f], Jagdish Krishnaswamy [b,c,g]

[a] School of Geography, Earth and Environmental Sciences, University of Birmingham, Edgbaston, Birmingham, B15 2TT, United Kingdom
[b] Ashoka Trust for Research in Ecology and the Environment (ATREE), Royal Enclave, Srirampura, Jakkur PO, Bangalore 560064, Karnataka, India
[c] Manipal Academy of Higher Education (MAHE), Manipal 576104, Karnataka, India
[d] Sikkim State Council of Science & Technology, Gangtok 737102, India
[e] Pforzheim University, Tiefenbronner Str. 65, 75175 Pforzheim, Germany
[f] Conservation Biology Institute, Oregon 97333, USA
[g] School of Environment and Sustainability, Indian Institute for Human Settlements, Bangalore 560080, India

ARTICLE INFO

Keywords:
Eastern Himalaya
Ecohydrology
Secondary forests
Streamflow
Transpiration
Tropical montane forests

ABSTRACT

Secondary tropical forests provide critical hydrological services through modulating transpiration and soil infiltration of precipitation. However, vegetation studies establishing direct mechanistic linkages between stand transpiration, soil moisture and streamflow are significantly lacking in tropical montane forests (TMFs) in Himalaya. We quantified the impact of diel and seasonal transpiration on catchment water balance and lean season streamflow in a broad-leaved evergreen secondary TMF in Eastern Himalaya. Stand transpiration (T) and streamflow (Q) were measured concurrently at one of the wettest (4500 mm yr^{-1}) and highest elevation (2100 m) sites worldwide to date. The observed daily transpiration rates (1.29±0.99 mm d^{-1}) were double the reported values from TMFs in relatively drier Central Himalaya but at the lower bound of TMFs globally. Moderate precipitation pulses (10–25 mm volume) followed by clear skies significantly increased stand transpiration. The proportional contribution of evaporative losses (50–77%) and stand transpiration (2–13%) to catchment water balance increased with the progression of the wet season. The phase lags between T, soil moisture (S) and Q were confounded by significant pre-dawn sap flux movement and the presence of secondary diel peaks. Transpiration was a significant predictor of streamflow in the dry season and, to a lesser extent, in the wet season. Thus, changes in vegetation cover and precipitation patterns will likely impact hydrological services from the regenerating secondary TMFs and the regional water security in the Eastern Himalaya.

1. Introduction

Tropical forests provide critical ecohydrological services by actively modulating water, carbon and nutrient cycles (Peña-Arancibia et al., 2019; Wohl et al., 2012). However, approximately half of the world's tropical forests are secondary in nature, having undergine historical human-induced degradation (Oberleitner et al., 2021). Recent literature has highlighted the growing importance of secondary forests in maintaining ecohydrological functioning and mitigating water security challenges in the tropical world (Heinrich et al., 2023; van Meerveld et al., 2021). Further, the functional diversity of secondary forests significantly alters the hydrological services through changes in canopy and soil properties (Wen et al., 2019). However, the existing research from secondary tropical forests has focused on the biogeochemical cycles, including carbon and primary productivity assessments, and literature on hydrological functioning remains scant, especially from data-scarce regions such as the Himalaya (Dib et al., 2023; Wen et al., 2019; Yang et al., 2023). The bulk of the tropical montane forests (TMFs) in the Himalaya are now secondary forests, which are defined as any regenerating forest patches after modifications or clear-felling of old-growth primary forests with significant differences in vegetation composition, density and functional diversity (Kanade and John, 2018; Kumar et al., 2023a; Ramakrishnan and Kushwaha, 2001). Secondary TMFs in the Himalaya are characterized by an assembly of different

* Corresponding author: Dr. Manish Kumar, Research Fellow, School of Geography, Earth and Environmental Sciences, University of Birmingham, Edgbaston, Birmingham B15 2TT, United Kingdom.
E-mail addresses: m.kumar.2@bham.ac.uk, manish.kumar@atree.org (M. Kumar).

https://doi.org/10.1016/j.ecohyd.2024.04.001
Received 16 August 2023; Received in revised form 19 March 2024; Accepted 3 April 2024
1642-3593/© 2024 The Author(s). Published by Elsevier B.V. on behalf of European Regional Centre for Ecohydrology of the Polish Academy of Sciences. This is an open access article under the CC BY license (http://creativecommons.org/licenses/by/4.0/).

functional groups, including long-lived pioneer and old-growth late--successional species, with contrasting growth rates and water-use strategies (Ghimire et al., 2014b; Kumar et al., 2023a). Secondary TMFs also have different under-canopy structures and hugely modified soil, which impact the key ecohydrological processes such as soil evaporation and infiltration of precipitation into the soil (Badu et al., 2022; Li et al., 2023; Pandey et al., 2023). Broad-leaved secondary forests form a significant portion (32.5%) of the total area under TMFs in Eastern Himalaya and are likely to have distinctly altered carbon and water cycles than primary forests (Bhutia et al., 2019; Kanade and John, 2018; Tiwari et al., 2023). The high water demand from these regenerating secondary forests dominated by pioneer species can exert significant pressure on limited soil moisture reserves and lean season streamflow (Kumar et al., 2023a; Wright et al., 2018).

Previous research highlights the vital role of broad-leaved TMFs in precipitation partitioning, runoff generation, and sediment transport in the Himalaya, where evapotranspiration can go up to 40% of the annual water budget (Ghimire et al., 2014b; Qazi et al., 2017; Sharma et al., 2007). However, few of these studies empirically estimate the transpiration component of evapotranspiration and instead rely on indirect methods using micro-meteorological data or water balance calculations (Ghimire et al., 2014b; Kumar et al., 2023a). Also, most studies operate at catchment-to-basin scales, and fewer studies have investigated the role of vegetation-driven evapotranspiration in headwater catchment processes (Ghimire et al., 2014b; Qazi et al., 2017; Sharma et al., 2007). At catchment scales, most of such studies have come from the Western and Central (Nepal) Himalaya and have focused on establishing linkages between stream characteristics and land-use forms, including the role of TMFs (Krishnaswamy, 2017; Sharma et al., 2007). At basin scales, studies have tried to quantify the relative contribution of glacial melt, snowmelt, runoff, and baseflow to the total discharge and undertand the impact of climate change in the Himalaya (Singh and Bengtsson, 2005; Singh and Kumar, 2010). With climate change, the region is projected to experience significant warming (0.8–1.2 °C decade^{-1}), increasingly drier winters and wetter monsoon and summer seasons, and their potential impact on the interactions between vegetation productivity and ecohydrological fluxes remains poorly known (Krishnan et al., 2019; Krishnaswamy et al., 2014; Kumar et al., 2021).

The literature on interactions between water and vegetation has been primarily focused on the ecophysiological aspects of transpiration, while a few have extended it to interactions between transpiration, soil moisture, and streamflow (Asbjornsen et al., 2011; Tashie et al., 2019; Wang et al., 2019). The extent of vegetative influence on soil moisture and streamflow varies considerably across micro-climatic conditions (water or energy limitations on plant productivity), catchment size, vegetation types, including the dominant functional groups and physiological traits such as rooting depths, which govern the ability of vegetation to access deeper subsurface moisture (vadose zone) and/or groundwater (Asbjornsen et al., 2011; Bonnesoeur et al., 2019; Evaristo et al., 2015; Gribovszki et al., 2010; Jasechko et al., 2013). For example, shallow-rooted trees may tap into the subsurface moisture, whereas deep-rooted tree species can access the water table directly and release it into the atmosphere through transpiration (Kumar et al., 2023a; Maeght et al., 2013). Conversely, Deng et al. (2021) report that access to karst groundwater, along with meteorological drivers, controlled sap flow. The loss of soil moisture or baseflow to the atmosphere, which otherwise could have contributed to streamflow, can significantly alter the local water balance and streamflow responses in a forested catchment (Barbeta and Peñuelas, 2017; Perry and Jones, 2017). A comprehensive review of hydrological signatures (McMillan, 2020) details up to 50 different signatures in streamflow, including diel and seasonal cycles, in response to various ecohydrological processes such as evapotranspiration, soil hydraulics, aquifer dynamics, hydrological portioning and human disturbances. In a simple dynamical catchment, diel and seasonal variations in transpiration and evapotranspiration can induce corresponding patterns in soil moisture and streamflow with significant phase lag (Bond et al., 2002; Kirchner et al., 2020; Moore et al., 2011; Woelber et al., 2018). Here, the phase lag between transpiration, soil moisture, and streamflow can either represent the transit time in large catchments or dynamical phase lag in small streams (Kirchner et al., 2020; Moore et al., 2011; Woelber et al., 2018). In contrast, the “two-water-worlds” hypothesis suggests that the water available for trees is potentially disconnected from the moisture stock that contributes to streamflow and that trees have limited access to groundwater (Berry et al., 2018a). However, the literature remains inconclusive on the presence of two moisture movement pathways with research evidence on trees accessing stream/groundwater in the valley or riparian zones (the riparian interception hypothesis) and/or evapotranspiration reducing the highly mobile surface soil moisture resulting in lower flow velocities (flowpath migration hypothesis) (Graham et al., 2013; McMillan, 2020). Both hypotheses, flowpath migration and riparian interception, hold potential in Himalayan TMFs with shallow soil strata, highly fractured geology, and significant dry seasons (Kumar et al., 2023a; Nanda et al., 2019). In a connected study from the Western Ghats in India, Nayak et al. (2023) predicted higher runoff generation in exotic wattle plantations and higher flood risks than native shola grasslands in response to higher precipitation intensities. However, the literature on interlinkages between vegetation and streamflow remains scarce from Himalayan TMFs (Bruijnzeel et al., 2011; Célleri and Feyen, 2009). The transpiration responses to changes in antecedent moisture and precipitation pulses is another emerging area of research, especially in regions with seasonal droughts (Burgess, 2006; Chen et al., 2014; Zeppel et al., 2008).

However, to the best of our knowledge, ecohydrological controls of vegetation-water use on streamflow have not been quantified and mechanistically explained in TMFs of the Himalaya. In a companion study at the same site, Kumar et al. (2023a) quantified the variabilities in intra-tree, inter-tree and inter-specific sap flow responses to microclimate in two long-lived pioneer species *Symplocos racemosa* and *Eurya acuminata*, and one old-growth late-successional species *Castanopsis hystrix*. They instrumented 13 trees of the three species with Granier’s thermal dissipations sap flow probes at variable depths and azimuthal directions to report five critical findings, which have significance for this research: (1) The fast-growing pioneers displayed 1.6–2.1 times higher sap flux densities (J, cm^3 cm^{-2} h^{-1}) than the late-successional species, (2) The species exhibited significant radial and azimuthal variability leading to bias in whole-tree sap flow (V, kg h^{-1}) estimation, (3) The species showed significant nocturnal sap flow (14% of total V) bulk of which occurred in the pre-dawn period (00.00–05.00 h), (4) Sunlight and Vapour pressure deficit (VPD) governed variabilities in winter and summer sap flow, respectively, and (5) The shallow-rooted pioneer species exhibited midday depression in V that was attributable to photosensitivity and diel moisture stress responses, whereas, the deep-rooted late-successional species transpired unaffectedly across the dry season, indicating access to deeper sub-surface moisture. They further suggested that midday depression in sap flow, and the resultant secondary peaks, are a characteristic of pioneer species which have evolved to transpire heavily at optimal conditions but remain highly sensitive to environmental extremes, such as high VPD and/or sunlight, and low soil moisture (Chiariello et al., 2006; Franco and Lüttge, 2002; Kumar et al., 2023a). Building upon the research and in a first attempt from Himalaya, the study aims to quantify the relative controls of vegetation-driven transpiration on lean (dry) season streamflow in broad-leaved evergreen secondary TMF of Sikkim, a representative region of Eastern Himalaya. The key questions addressed in the study are: (a) What is the role of vegetation-driven evapotranspiration in the catchment water balance? and (b) How does transpiration impact diel and seasonal streamflow variability in an East Himalayan secondary TMF? We hypothesized that stand transpiration, fueled by the dominance of fast-growing pioneer species transpiring heavily in wet and tropical conditions, will be a significant component of the catchment water balance. Further, in seasonally dry winter, high transpiration rates would negatively affect streamflow with increased amplitude of diel

streamflow due to a combination of riparian interception and flowpath migration hypotheses.

2. Material and methods

2.1. Study site and forest stand description

We instrumented a headwater micro-watershed in the Fambong-Lho Wildlife Sanctuary (FWS, N27.583, E88.933), which forms the upper catchment of the Lay Khola, a tributary of the Teesta River in East Sikkim, India (Fig. 1). The regional geology belongs to the Gorubathan group, mainly comprising alternating bands of phyllite-quartzites overlain by micaceous schist on the ridge top. The instrumented micro-watershed has a catchment area of 0.16 km^2 (16.1 hectares) with an elevational range of 2100 - 2400 m above sea level (masl). The mean annual precipitation is 4650±120 mm, with temperature fluctuating between a yearly maximum of 24°C to a minimum of −2°C (2013–2015) (Supplementary Figure A1). At the site, the lower latitude (27–28°) and proximity to the south-west Indian monsoon favour tropical climatology with three distinct seasons: winter (November - February) with sunny days, freezing nights, sporadic snowfall and low evapotranspiration; summer (March-May), characterised by warm and cloudy days, high evapotranspiration and substantial pre-monsoon precipitation occurring in the afternoon, and monsoon (June - October) with high humidity, low evapotranspiration and concentrated precipitation occurring in the late-night to early morning period, a phenomenon unique to the Himalaya (Barros and Lang, 2003; Kumar et al., 2021; Pandey et al., 2016). During the study, the winter (December 2013 – February 2014) marked the dry season with sunny but cold days and sub-zero night temperatures. The summer (March 2014 – May 2014) saw increased day length, predominantly afternoon precipitation, abundant moisture, warmer temperatures, and higher plant productivity (Kumar et al., 2023a).

The forest stand falls under the FWS, which was declared as a protected area (PA) four decades ago (1984) after experiencing considerable human-use, including selective harvesting of hardwood species for timber and clear-felling in patches for agricultural purposes (Sudhakar et al., 2008). Post-1984, all harvesting was banned and the forest was left to regenerate naturally. The forest stand represents early successional secondary East Himalayan broad-leaved wet montane forests (Kanade and John, 2018; Kumar et al., 2023a; Sudhakar et al., 2008) and as mid-altitude oak forests dominated by *Castanopsis hystrix* (Bhutia et al., 2019). The forest stand is characterised by (a) the dominance of broad-leaved evergreen species and (b) a sub-tropical montane climate with high precipitation and strong diel and seasonal temperature. The vegetation data were derived from four 1000 m^2 (100 m X 10 m) vegetation survey plots, which enumerated 16 species belonging to 12 families and a total of 321 trees above 10 cm diameter at breast height (DBH) (Bhutia et al., 2019; Kumar et al., 2023a). The total basal area of the forest stand was 37. 23 m^2 ha^{-1}, and the stand density was 505 tree ha^{-1}. The average tree DBH was 0.23±0.21 m, and the size class

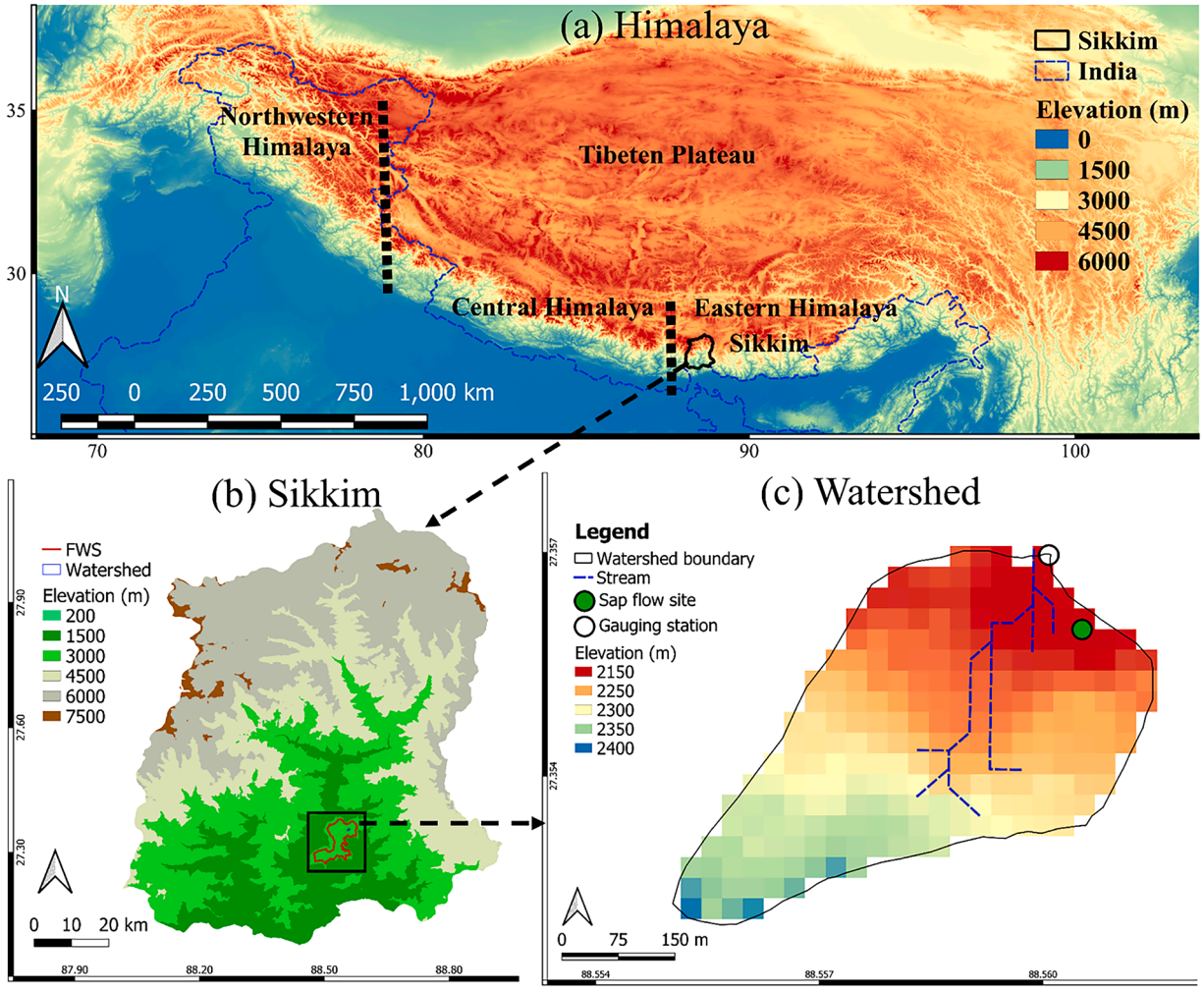

Fig. 1. Study area map showing (a) Digital elevation model (DEM) map of Himalaya and Sikkim within India; (b) the location of Fambong-Lho wildlife sanctuary (FWS) and the instrumented watershed within Sikkim; and (c) DEM of the delineated watershed of the first-order stream in FWS with the location of the sap flow instrumentation site, and precipitation and stream gauging stations.

histogram showed a reverse "J"-shaped distribution, indicating an uneven-aged forest with an abundance of small-sized trees (40% trees belonging to 0.1–0.14 m DBH) (Supplementary Figure A2b) (Bhutia et al., 2019). Moderate Resolution Imaging Spectroradiometer (MODIS) Leaf Area Index/FPAR (MCD15A3H v006) was used to extract the Leaf Area Index (LAI, dimensionless) and Normalized Difference Vegetation Index (NDVI, unitless) was computed from the infrared and near-infrared bands of MODIS-Terra Surface reflectance (MOD09A1 v006) for the study site (Myneni et al., 2015; Vermote, 2015). The average stand LAI was 1.54±1.51, with a maximum of 7.1 in September 2014, whereas NDVI peaked (0.78) in October 2014 (Supplementary Figure A1f). The species composition is dominated by the three species: *Symplocos racemosa, Eurya acuminata,* and *Castanopsis hystrix*, which form 58.3% of total stand trees and 38.3% of the total basal area (Bhutia et al., 2019; Kumar et al., 2023a). The short-statured canopy (3–8 m tall) is dominated by pioneer species like *S. racemosa* and *E. acuminata*, while the older remnant trees *C. hystrix* stood out as emergent (Bhutia et al., 2019; Kumar et al., 2023a). A detailed description of the forest stand and sap flow responses of the three dominant species to environmental conditions has been provided by Kumar et al. (2023a)

2.2. Data collection

2.2.1. Sap flux measurements and scaling from whole-tree sap flow to stand transpiration

Sap flux density was measured using Granier's thermal dissipation method (TDP) probes in 13 trees of the three dominant species, *S. racemosa, E. acuminata,* and *C. hystrix*. For detailed methodology for TDP probe manufacturing, instrumentation, and scaling from individual probes to whole-tree sap flow, please refer to Kumar et al. (2023a). The thermal dissipation method applies to a wide range of species and is easy to manufacture locally at low costs (Davis et al., 2012; Flo et al., 2019; Granier, 1987; Lu et al., 2004). The volumetric sap flow from the 13 trees of the three species was scaled to stand transpiration (T, mm h^{-1}) using the data from vegetation plots and sapwood area as the scalar. Existing sap flow literature suggests tree-size as the most used scalar for tree-to-stand transpiration, provided the species selection for the original sap flow data is representative of the forest stand (Asbjornsen et al., 2011; Berry et al., 2018b; Forrester et al., 2022). However, most existing studies come from relatively homogenous or well-studied long-term experimental plots, which lend robustness to the estimated stand T. Even then, the estimation bias in scaling from a single probe to a whole tree and from whole-tree to a forest stand is well-known in sap flow studies (Asbjornsen et al., 2011; Kumagai et al., 2005a). We minimised the probe-to-tree-level scaling bias by focusing on radial and azimuthal variabilities in the 13 sampled trees (most sap flow studies sample <9 trees) (Kumar et al., 2023a; Mackay et al., 2010). This is the first study on vegetation-water-use from the region and the forest type. In the absence of prior studies, we accounted for the inter-specific variation in the tree-size and plant water-use by sampling for the three most dominant species while maintaining representativeness across the two main functional groups: long-lived pioneer species and late-successional species (Kumar et al., 2023a).

A five-step approach was adopted to scale sap flow (V in kg h^{-1}) from the instrumented trees to the stand level using tree diameter measured at breast height (DBH) as a scalar (Chiu et al., 2016). First, a non-linear least squared (NLS) regression model (intercept = 0.112, power coefficient = 0.857, $P < 0.001$) was fitted between tree diameter (DBH in m) and total sapwood area (SWA in m^2) of the 13 trees (Supplementary Figure A3). A recent meta-analysis of global sap flux studies suggests that the assumptions of linear fit between tree size and sapwood area for scaling whole-tree sap flow are limited to homogenous stands, and studies with large trees should explore non-linear regression models (Forrester et al., 2022). Thus, despite being limited by 13 instrumented trees, the observed non-linear fit between the sapwood area vs. tree diameter relationship was ecologically appropriate for the secondary forest stand being investigated. It is also in accordance with observations of linear increase in sapwood area until an optimal tree size, after which heartwood formation leads to relatively lower incremental growth of sapwood area per unit increase in tree size (Berry et al., 2018b; Forrester et al., 2022). Similar studies on individual tropical species report a non-linear rise in sapwood area with tree diameter, which complemented our DBH-sapwood area relationship at the study site (Lehnebach et al., 2017; Uyup et al., 2023; Yang and Hazenberg, 1991). In the next step, the NLS regression model coefficients were used to compute SWA from DBH for each tree (>10 cm DBH) sampled in the vegetation plots. Third, the instrumented trees were categorised into four DBH classes for stand tree-size representativeness: < 0.15 m (small-sized trees, $N = 2$), 0.15–0.19 m (medium-sized trees, $N = 4$), 0.20–0.24 m (medium-large-sized trees, $N = 4$), and > 0.25 m (large-sized trees, $N = 3$) (Supplementary Figure A2a). The average sap flux density per class (J_{avg}) was computed by normalising the V of each instrumented tree by its SWA and averaging for each class. Fourth, all trees >10 cm DBH sampled in the vegetation plots were categorised into the above-mentioned DBH classes: < 0.15 m ($N = 80$), 0.15–0.19 m ($N = 40$), 0.20–0.24 m ($N = 39$), and > 0.25 m ($N = 43$) (Supplementary Figure A2b). Whole-tree sap flow (V) was estimated for each tree in the forest stand by multiplying the corresponding J_{avg} of the diameter class with its SWA. Fifth, stand transpiration (T in mm h^{-1}) was computed by aggregating hourly V for all trees in the vegetation plots and dividing it by the total plot area (4000 m^2). We initially attempted gap-filling through a generalised linear regression model to predict the response of tree sap flow (V) to changes in micro-meteorological drivers such as solar radiation and Vapor pressure deficit (VPD), details of which are available in Kumar et al. (2023a). While the model results were very insightful in understanding the processes and interactions, the overall predictive power of the model was low for the three species ($0.08 < r^2 < 0.41$). The predicted sap flow failed to replicate key diel features in the observed sap flow, i.e. the early-morning transpiration onset and mid-day depression. Thus, gap-filling of the missing data for the stand transpiration was consciously avoided. After quality checks, a total of 114 days (70% of total sampling days) of stand transpiration data was used for final analysis, including 74 days of concurrent data for T and environmental variables (P, S, Q and E_0) between November 2013 to May 2014 (Fig. 2).

2.2.2. Environmental and hydrological measurements

An automated stilling well fitted with a capacitance water level recorder (Dataflows Systems LTD, New Zealand) was installed on the first-order stream draining the micro-watershed. Streamflow (Q, mm h^{-1}) was computed from the water-level using a stream-specific rating curve and catchment area. We used the slug injection (salt-dilution) method, which is most suitable for small (first-order) streams, to estimate stream discharge and develop the rating curve (Supplementary Figure A4) (Nayak et al., 2023). On-site Precipitation (P, mm h^{-1}) was recorded using an automated tipping-bucket rain gauge. An on-site automatic weather station (AWS) (Vantage-pro Davis Net, USA) was installed to record meteorological parameters, i.e. incoming short-wave radiation (R_s in kW m^{-2}), air temperature (T_{emp}, °C), wind speed (u in m s^{-1}), and relative humidity (R_h in%) at high frequency (10 mins resolution) (Kumar et al., 2023a). Reference evapotranspiration (E_0, mm h^{-1}) was computed from the meteorological data following FAO's Penman-Monteith method (equation 6 of FAO56PM and Allen et al. 1998). Soil water potential was recorded (10-minute resolution) at 10 cm incremental depths from the topsoil to up to 30 cm depth using granular matrix-based (watermark) sensors (Virtual Electronics, Roorkee) and converted to volumetric water content using the site-specific van Genuchten water retention curve (developed using Rosetta software, Schaap et al., 2001). Total soil moisture (S, mm) was computed for the topsoil (0–30 cm depth) using the trapezoidal method, and stray missing values were gap-filled through a 3-step moving-average window (Nachabe et al., 2005). Soil cores were collected at six locations at the

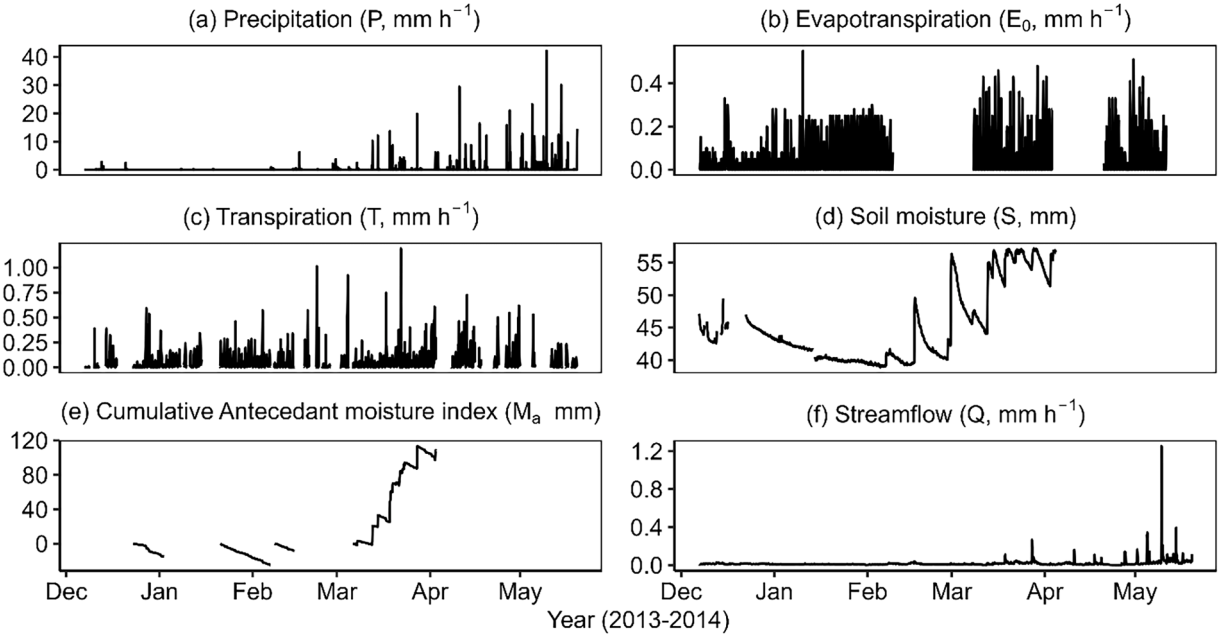

Fig. 2. Time-series plots of the raw daily data of the study variables from winters (December) to summers (April): (a) Precipitation (P, mm h^{-1}), (b) Evapotranspiration (E$_0$, mm h^{-1}), (c) Stand Transpiration (T, mm h^{-1}), (d) Soil moisture (S, mm), (e) Cumulative antecedent moisture index (M$_a$, mm), and (f) Streamflow (Q in mm h^{-1}).

site, varying from 20 to 90 cm depth (mean±SD, 50±28 cm) till we hit the bedrock. The cores were separated into 10 cm blocks, and depth-wise changes in particle size distributions were determined using sodium hexametaphosphate as the dispersing agent based on Bouyouco's hydrometer method (Bouyoucos, 1928). A Mini disc infiltrometer (Decagon Devices, Inc., Pullman, WA) was used to collect soil infiltration measurements ($N = 10$) on a flat surface after removing any leaf litter present, and unsaturated soil hydraulic conductivity was estimated (Nanda et al., 2019; Zhang, 1997).

2.3. Data analysis

We first looked at the impact of moisture input (precipitation pulses) on T and its relative importance to the catchment water balance. Then, the diel cycles of T, S and Q were examined visually and through lag regression anakysis to understand their daily phase difference as an indicator of catchment interconnectivity. Lastly, the interactions were quantified using step-wise lag regression models (run separately for wet and dry periods) to understand the relative influences of precipittaion, transpiration and micro-climate on streamflow. The data processing, analysis, and visualisation were done in the R programming software (version 4.3.2) (R Core Team, 2024).

2.3.1. Catchment water balance

In steep mountain catchments with shallow and sloped aquifers, the soil profile acts as a transient storage supporting the movement of moisture between aboveground (vertically downward moving infiltration from precipitation and upward moving moisture-uptake for transpiration and evaporative losses) and belowground stocks (groundwater recharge to aquifer) (Fan et al., 2023; Kumar et al., 2023a). Due to logistical limitations, we could not monitor the soil moisture at depths greater than 30 cm from the ground and assumed that any downward flux contributed to the aquifer recharge, which provides baseflow to the stream. Thus, any changes in the aquifer storage were assumed to be linearly reflected in streamflow. The catchment water balance was estimated for the events using simple mass balance assuming non-leaky aquifer conditions using equation 1, where ΔS is inclusive of the change in topsoil moisture (0–30 cm depth), Q is streamflow inclusive of changes in deep soil moisture and shallow aquifer storage (D. McJannet et al., 2007), and E_{loss} represents combined evaporative losses through physical processes such as air and soil evaporation, forest canopy and floor-based interception losses, and changes in tree surface moisture (bark, lichens mosses, etc.), excluding transpiration (T).

$$P = E_{loss} + T + \Delta S + Q \quad (1)$$

2.3.2. Impact of precipitation pulses on stand transpiration

The daily precipitation time-series was analysed to understand the impact of precipitation pulses on stand transpiration. Precipitation events were identified based on an interevent period of 24 h, event volume of >2.5 mm and duration, including the start of the precipitation to 24 h after the last recorded precipitation. All events longer than two days in duration and a total precipitation volume above 2.5 mm were considered precipitation pulses (Zeppel et al., 2008). Precipitation event volume denotes the extent of moisture input to a system and thus was preferred over precipitation intensity. Despite data gaps in the environmental parameters, we included all the events for which at least the changes in T were present for interpretation. The percentage changes in T, Q, E$_0$, R$_s$ and D were estimated as differences between their respective values on the day of the precipitation event and the day after (Chen et al., 2014).

2.3.3. Diel cycles of stand transpiration and other variables

In a typical time-series of Q or S, the trend component characterises the long-term changes across seasons and years and can confound the cyclic component, which is inferred here as the diel cycles. Thus, both Q and S were de-trended (*stlplus* function, package *stlplus*) to remove excessive noise in the diel cycles from the trend components (Kumar et al., 2023a). The filtered diel signals in S (S_{diel}) and Q (Q_{diel}) were computed for precipitation-free days to avoid the confounding effects of precipitation, and their diel patterns were compared with raw data to check for artificial peaks, if any (Supplementary Figure A5). The strength of the diel signal in Q was quantified as the ratio of the amplitude of the diel cycle ($Q_{daily.amp}$, in mm) to average daily Q, where $Q_{daily.amp}$ was computed as the half of the difference between the daily maxima and minima for the contiguous rainless periods longer than five

days. Lundquist and Cayan (2002) suggested a 30% significance threshold for $Q_{daily.amp}/Q$, although the threshold is likely to vary with catchment size, gradient and variability in stream velocities across different seasons (Wondzell et al., 2007). $Q_{daily.amp}$ was corrected for measurement error (0.008 m) induced by diel changes in ambient temperature, a known source of error in the capacitance water-level recorders used in the study (Larson and Runyan, 2009). The measurement error for the capacitance probe at the field site was derived empirically using a standing water column experiment with a fixed water level. To understand the seasonal variability in the significance of the diel cycle of Q to overall Q, we estimated the ratio of the variance of the diel component of streamflow ($Q_{dielvar}$) to the variance of streamflow (Q_{var}), computed for contiguous rainless periods longer than five days. A relatively higher variance ratio denotes an increase in diel amplitudes when the corresponding streamflow remains stable over the period, whereas a low variance ratio implies that the changes in streamflow overshadow the corresponding changes in the diel cycle.

2.3.4. Lag correlation analysis between transpiration, soil moisture and streamflow

Lag correlation analysis quantifies the correlation between variables that are at temporal lag with each other in a physical environment, a characteristic in ecohydrological interactions, and was preferred due to the observations of strong autocorrelations and secondary peaks in the variables (Kumar et al., 2023a; Moore et al., 2011). The lag (in hours) between the following combinations, T vs. S, S vs. Q, T vs. Q and P vs. Q was computed for each day using the cross-correlation function (*ccf* function in R). The *ccf* function provides default confidence intervals based on the quantiles (5%) of a standard normal distribution and does not account for the statistical properties of the data. Thus, as a conservative approach, we filtered the results for events with an auto-correlation coefficient (ACF) value higher than ±0.4 for further interpretation. Positive (negative) autocorrelation coefficient (ACF) values signified that a high (low) value of the driver variable was followed by a high (low) value of the response variable after the corresponding lag hours (Kumar et al., 2023a; Nayak et al., 2023).

2.3.5. Step-wise lag regression models for streamflow

In order to assess the relative influences of transpiration and rainfall on streamflow, a combination of a temporal lag model and the Generalised least squares (GLS) regression model (*gls* function, package *nlme*) with the suitable correlational structure was used in a step-wise manner (Krishnaswamy et al., 2012; Kumar et al., 2023a). The environmental variables showed significant temporal autocorrelation and lag with stand transpiration, necessitating the temporal lag model. The GLS regression method estimates the maximum likelihood of the regression coefficients using generalised least-squares and is most suitable for analysing time-series data with autocorrelational structures (Krishnaswamy et al., 2012; Kumar et al., 2023a). The streamflow GLS model used Q as the response variable and T, S, Antecedent moisture index (M_a), and P as predictor variables. M_a was used as a proxy for the antecedent state of moisture in the system and estimated using equation 2, where P_{cum}, T_{cum}, and Q_{cum} are cumulative sums of P, T, and Q, respectively (Potts et al., 2006).

$$M_a = P_{cum} - T_{cum} - Q_{cum} \quad (2)$$

The streamflow GLS models were separately run for the rainless (December –February) and rainy (March-May) periods with first-order autoregressive structure (corAR1), which is considered suitable and parsimonious for streamflow modelling (Krishnaswamy et al., 2012; Pinheiro and Bates, 2006). Before running the models, S and M_a were normalised by subtracting the daily mean, tested for collinearity, and then contiguous subsets longer than five days and without any missing values were extracted.

In linear regression, an interaction term is very useful in cases where the effect of an independent variable on the response variable is affected by the value of another independent variable. In headwater catchments, both soil moisture and transpiration can independently affect streamflow through recharge (S contributing to Q gravimetrically) and abstraction (tree roots accessing groundwater directly), respectively (Asbjornsen et al., 2011; Kirchner et al., 2020; Moore et al., 2011). However, they may also act in a continuum where transpiration draws the moisture from the soil, which could have potentially contributed to streamflow. In such a case, soil moisture acts as a buffer between transpiration and streamflow, and any changes in soil moisture will affect both T and Q independently, as well as the relationship between T and Q. Thus, we used the interaction term between S and T (S*T) as the predictor variable to assess the effects independently and interactively. The interaction term S*T was the predictor variable for the precipitation-free periods (Equation 3), whereas P, M_a, and the interaction term S*T were the predictor variables for the period with precipitation (Equation 4), where β and γ are the regression coefficients, for equation 3 and equation 4, respectively.

$$Q = \beta_0 + \beta_1 * S + \beta_2 * T + \beta_3 * S * T + \epsilon \quad (3)$$

$$Q = \gamma_0 + \gamma_1 * S + \gamma_2 * T + \gamma_3 * S * T + \gamma_4 * P + \gamma_5 * M_a + \epsilon \quad (4)$$

If the individual variables and their interaction were found statistically significant ($p < 0.05$), we interpreted the interaction term only. However, if the interaction term was statistically significant but the individual variables were not, we still interpreted the individual terms alongside their interaction term following the hierarchical principle.

Owing to the observed lag between the driver variables, the GLS model was run using a reconstituted time-series dataset, where each driver variable was first tested for the lag in a step-wise manner (Krishnaswamy et al., 2012). For each driver variable, firstly, the highest significant lag (L in hours, at ACF >= |±0.4|) between the driver and response (Q) variable was calculated for each contiguous subset using the *ccf* function. Then, the driver variable was lagged from zero lag to L hours to develop a multiple lagged time-series for each driver variable. Multiple linear regression models (MLRs) were fitted between Q and the lagged time-series the driver variable, and the time-series with the lowest significant lag ($p \leq 0.05$) was chosen. The MLRs were used as an additional step to ensure that the lagged time-series was most suited to Q. The procedure was repeated for the other driver variables, and the final time-series set was used to run the GLS model (Kumar et al., 2023a). We also tested the impact of adding correlational structure to the GLS model by running the GLS model separately with and without correlation structures and comparing the results using the Analysis of variance (ANOVA) test. The GLS model with the lowest Akaike Information Criterion (AIC), higher likelihood ratio, and significance was chosen for interpretations of variables with significant coefficients ($p \leq 0.05$) (Krishnaswamy et al., 2012). The Gupta-Kling Efficiency (KGE) score was used to assess the model performances by comparing the observed and predicted time-series of Q (Gupta and Kling, 2011).

3. Results

3.1. Stand transpiration and environmental characteristics

Average stand transpiration (T) ranged from 0.02 to 5.28 mm d^{-1}, approaching a maximum of 5.28 mm d^{-1} and mean (±standard deviation) of 1.29±0.99 mm d^{-1} (Fig. 2c). T exceeded the 75th percentile (1.9 mm d^{-1}) on 25% of total days ($n = 29$ days) and the 90th percentile (3.2 mm d^{-1}) on 10.5% of total days ($n = 12$ days). The average T in summer (1.76±1.3 mm d^{-1}) was 34% higher than in winter (1.16±0.8 mm d^{-1}). December to February was marked as the dry season with little precipitation, low E_0, depleting soil moisture and lowest streamflow. From March onwards, soil moisture recovered with the initial summer showers, followed by heavier summer precipitation in April and May, moderate E_0 and flash responses in streamflow. The texture analysis shows that the forest soil is well-drained sandy loam (Supplementary

Figure A6a). The average available water holding capacity was 16±8%, which increased with the soil depth reaching a maximum of 21±9% at 40 cm depth (Supplementary Figure A6b). The average unsaturated soil hydraulic conductivity was relatively low (mean±SD, 7.3 ± 4.8 mm h^{-1}). The precipitation intensity at the site was below the mean unsaturated hydraulic conductivity till the 90th quantile, with a maximum of 24 mm h^{-1} (Supplementary Figure A7).

3.2. Role of transpiration in catchment water balance

In the absence of continuous *in-situ* E_0 and T observations for the whole year, water balance was estimated for the study period when concurrent data was present for all the parameters (n = 72 days). The total precipitation (P, 157 mm) was partitioned into high transpiration (T, 86.8 mm, 55.3% of P), minor changes to soil moisture storage (ΔS, 2.2 mm, 1.4% of P), and streamflow (Q, 23.4 mm, 14.9% of P), and the remainder was attributed to other evaporative losses (E_{loss}, 44.5 mm, 28.4% of P). As seen in Fig. 2d, the fully saturated soil moisture reserve dips to its lowest point in mid-February and is replenished back to its original levels by the pre-monsoon precipitation in March-May 2014. Thus, despite significant fluctuation in soil moisture levels, i.e. the difference between maximum and minimum soil moisture over the study period was 18 mm, the net change (ΔS) was negligible. Event-based catchment water balance was computed for four precipitation events ranging from 13 to 82 mm in volume and 1–6 days in duration (Fig. 3). The events mark the first rains in the summer after a prolonged dry winter (Fig. 2a). The first two events (Event 1 and 2) were initial showers of a few hours each and low antecedent moisture (M_a, 0.1 ± 0.8 mm). They mainly contributed to the soil moisture storage (ΔS) and high evaporative losses (E_{loss}) while barely contributing to streamflow (Q). However, the later events, post soil saturation and at higher M_a (48±33 mm), marked a further increase in evaporative losses (E_{loss}) but also a marked increase in T and streamflow (Q). T as a fraction of total evapotranspiration losses ($T + E_{loss}$) varied from 5 to 15% across the four events.

3.3. Impact of precipitation on stand transpiration

A total of nine precipitation pulses were identified during the study period, including eight events in summer, while one small-sized precipitation (2.5–10 mm) was in winter (Supplementary Table A1). The event volumes ranged from 5.3 to 82.2 mm with a mean precipitation volume of 35.9 ± 29.1 mm. On average, T almost doubled (93±110%) after the three medium-sized precipitation pulses (10–25 mm) and increased by one-third (29±28%) after the four large-sized pulses (≥25 mm) (Table 1). Incidentally, the days with unusually higher values of T after the medium-sized precipitation pulse (10–25 mm) were accompanied by a moderate increase in evaporative demand (moderate E_0 and M_a), sunlight (Rs, 48±41%), and VPD (29±63%). In contrast, large precipitation pulses (≥25 mm) were followed by increased sunlight availability (79±45%) and a moderate decline in VPD (−14±23%), an increase in evaporative demand (E_0, 67±58%) and low antecedent moisture conditions, leading to a proportionately moderate increase in T. However, T declined by −64±7% after the two small precipitation pulses (2.5–10 mm), despite the rise in VPD (74±118%) and decline in antecedent moisture conditions. Expectedly, the increase in the size of precipitation pulses led to an exponential increase in Q, whereas the effect on S was highest after mid-sized events.

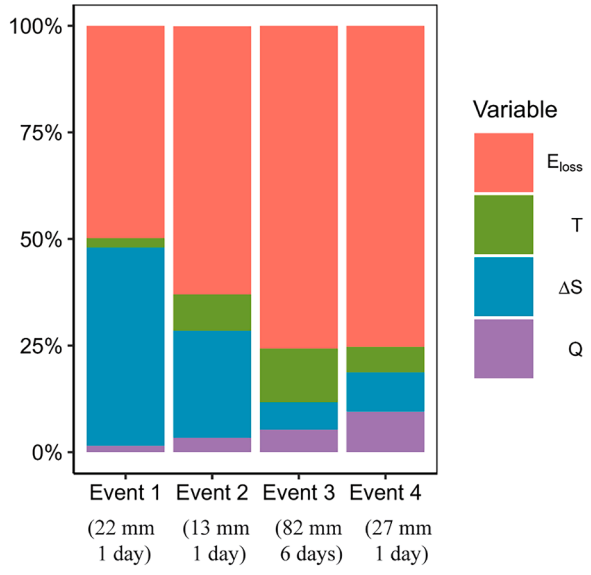

Fig. 3. Barplot shows percentage fractions of water balance components for different precipitation events.

3.4. Diel cycles in stand transpiration, evapotranspiration, soil moisture and streamflow

The changing dynamics between soil-plant-atmosphere-streamflow can be closely observed in Fig. 4, which shows continuous time-series plots of E_0, T, S, S_{diel}, Q, and Q_{diel} for a 17-day rainless period in the winter. The days have consistent E_0 with a modular peak at 1300–1400 h and negligible E_0 during the night (Fig. 4a). Conversely, during half of the days, T showed bi-modal peaks, characterised by early onset (pre-dawn), a minor peak early in the morning (0700 h) and the major peak coinciding with E_0 at 1400 h. On other days, T showed a unimodal peak at 1400 h (Fig. 4b). S declined linearly over the period, whereas Q showed an abrupt decline in the middle (Fig. 4c and 4e).

In the first half, S_{diel} had afternoon peaks (1500 h) and early morning (0400–0800 h) troughs (Fig. 4d). In this period, T showed bi-modal peaks, and the pre-dawn onset of T coincided with the decline of S_{diel}. Afterwards, S_{diel} recovered sharply during the mid-day trough in T, albeit with 2-hours lag time, but started to decline again as T gained momentum for the second peak. In the latter half, the afternoon peaks in S_{diel} shifted to noon (1200 h) with an increase in the amplitude of diel fluctuations, which could be attributed to the lesser number of days with bimodal peaks in T during the second half. In the first half, Q_{diel} had bi-modal peaks in the morning (0800 h) and evening (1700 h) and troughs in the pre-dawn (0400 h) and mid-day (1200–1500 h) periods, which shifted to unimodal peaks in morning (0800 h) in the later half (Fig. 4f). S_{diel} and Q_{diel} were out of sync, with the peak in the former coinciding with the trough in the latter (Supplementary Figure A5). However, the peak in E_0 and the second peak in T coincided with the peak in S_{diel} and the trough in Q_{diel}.

The relative size of diel cycles of streamflow (Q) to the overall Q was computed over nine contiguous rainless periods (longer than five days) to understand if the diel cycles were significant (Fig. 5a). The ratio of the variance of the diel component of Q (Q_{diel}) to the variance of Q ranged from 1.3 to 27% with a mean±SD of 7.1 ± 8%. The variance ratio increased from winter (4 ± 3.5%) to summer (14±12%), peaking in March (27%) (Fig. 5a). The low values in April (7 ± 0.4%) were preceded by significant precipitation events. Similarly, the ratio of the diel amplitude of Q ($Q_{daily.amp}$) to daily Q (Q_{daily}) increased from 0.8 to 76% with a mean±SD of 23±11% reaching the high points in March (34 ±13%) and November (28±14%) coinciding with extended rainless periods (Fig. 5b).

3.5. Lag correlation between transpiration, soil moisture and streamflow

The simple correlation tests between T, soil moisture and streamflow variables yielded low correlations due to temporal lags between the diel cycles of different variables. The cross-correlation analysis accounted for the shifting lags between T, S, P and Q with considerable variation

Table 1
Percentage changes (real values in bracket) in Reference Evapotranspiration (E_0), Net radiation (R_s), Vapour pressure deficit (VPD), Stand Transpiration (T), Soil moisture (S), Cumulative antecedent moisture index (M_a) and Streamflow (Q) after precipitation pulses of varying sizes (SE = standard error, N = Number of events).

Precipitation (P) size classes (mm, mean ±SE, N)	ΔR_s in% (kW m^{-2} ±SE)	ΔVPD in% (unitless^{-1} ±SE)	ΔE_0 in% (mm d^{-1} ±SE)	ΔT in% (mm d^{-1} ±SE)	ΔS in% (mm ±SE)	ΔM_a in% (mm ±SE)	ΔQ in% (mm d^{-1} ±SE)
2.5–10	−3	74±118	−3	−64±7	1 ± 2	−1444	−3 ± 1
(7 ± 1, N = 2)	(−0.001)	(0.03±0.04)	(0.01)	(−0.55±0.3)	(−0.6 ± 0.9)	(2.86)	(−0.01±0.002)
10–25	48±41	29±63	51±44	93±110	13±9	356 `±326	39±22
(20±4, N = 3)	(0.04±0.03)	(0.01±0.04)	(0.55±0.43)	(0.24±0.36)	(6.1 ± 3.9)	(12.4 ± 5.2)	(0.07±0.06)
>25	79±45	−14±23	67±58	29±28	3 ± 4	39±41	209±218
(62±11, N = 4)	(0.03±0.02)	(−0.02±0.02)	(0.39±0.36)	(0.02±0.4)	(1.53±2.3)	(13.4 ± 15.3)	(0.3 ± 0.33)

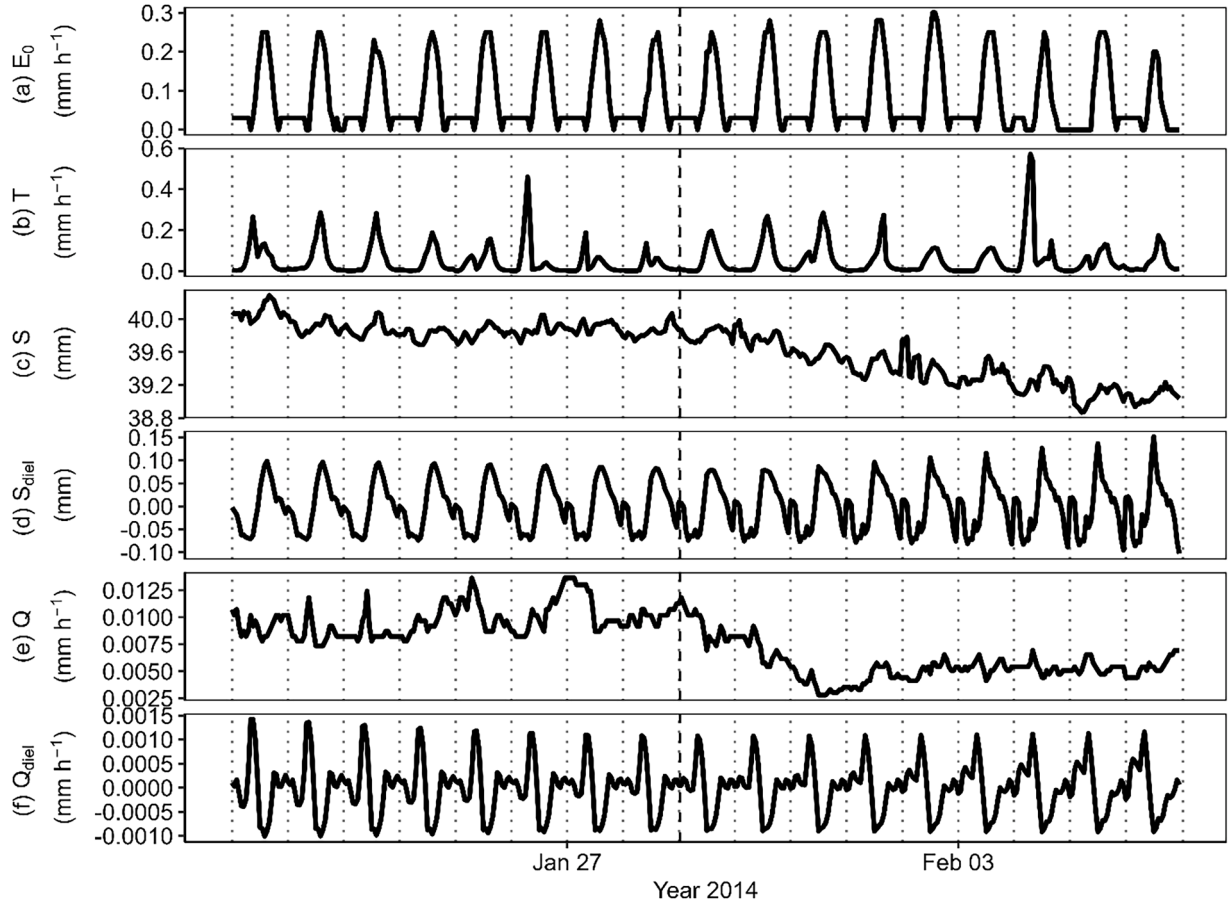

Fig. 4. Time-series plots of SPAFC variables for a rainless 17-day contiguous period in winters: (a) Evapotranspiration (E_0), (b) Stand transpiration (T), (c) Soil moisture (S), (e) Streamflow (Q), and (d) S_{diel} and (f) Q_{diel} are the diel components of soil moisture and streamflow, respectively. The vertical dotted lines mark 0000 h time for each day and the vertical dashed line marks the mid-point of the dataset shown.

observed across the winter (dry) and summer (wet) periods (Fig. 6).

On half of days in the winter (N = 18), the diel peak in S lagged the diel peak in T by −2.2 ± 4.1 h with strong positive correlations (0.66 ±0.1). However, on the remaining days in winter (N = 16), the diel trough in S lagged the peak in T by −1.5 ± 6 h with strong negative correlations (−0.55±0.1). In summer, on most days (N = 14), the trough in S lagged peak T by −6 ± 3 h with negative correlations (−0.55±0.1), whereas, with the advent of rains, the peak in S lagged peak T by −1.3 ± 7.6 h (N = 11 days) with positive correlations (0.6 ± 0.16). Similarly, on most days in the winter, the diel peak in S lagged the peak Q by 1.3 ± 5 h (N = 22 days) and with positive correlations (0.56±0.1), whereas on remaining days (N = 9), the trough in Q lagged the peak S by 0.11±2 h and negative correlations (−0.6 ± 0.1). However, in the summer, with increased wetness, peak S lagged peak Q by an increased lag time (2.9 ± 3 h, N = 15) with positive correlations (0.7 ± 0.16). However, on the remaining days, the trough in Q lagged the peak S by −3.3 ± 5.4 h and negative correlations (−0.58±0.1). On most days in the winter, the peak in T lagged the peak Q by 1.3 ± 5 h (N = 20 days) and with positive correlations (0.56±0.1), whereas on remaining days (N = 14), the peak in T lagged the trough in Q by 1.3 ± 4 h and negative correlations (−0.6 ± 0.1). However, with increased transpiration rates in the summer, peak Q lagged peak T by an increased lag time (−1.6 ± 6 h, N = 14) with positive correlations (0.7 ± 0.1). However, on the remaining days in the summer (N = 12), the trough in Q lagged the peak T by −2.1 ± 2.8 h and negative correlations (−0.64±0.1). Expectedly, Q peaked −1.5 ± 0.7 h after the peak precipitation (P) with positive correlations (0.43±0.01) in the winter (N = 2), and the lag time reduced to −0.9 ± 2.7 h with strong positive correlation (0.7 ± 0.14, N = 10) in the summer.

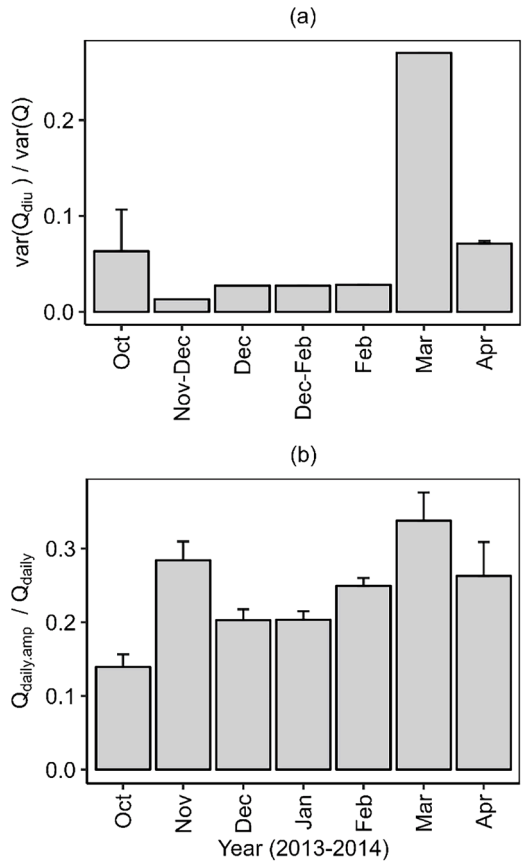

Fig. 5. Barplots showing (a) the mean ratio of the variance of the diel component of streamflow (Q_{diel}) and streamflow (Q), and (b) the mean ratio of the diel amplitude of Q ($Q_{daily.amp}$) to mean daily Q (Q_{daily}), computed for contiguous rainless periods in the hydrological year 2013–2014. The error bars represent standard errors.

3.6. Step-wise lag regression model for streamflow

The streamflow GLS model was fitted to four rain-free periods from November to May, including three in winter (6–17 days in length) and one in summer (27 days in length) (Table 2). The streamflow GLS model with corAR1 correlation structure had significantly lower AIC than the GLS model without any correlational structure and was chosen for model interpretation. In summer, P lagged by an hour as per lag regression analysis and the final timeseries was suitably lagged. The streamflow GLS model performed better in winter with higher concurrence between predicted and observed Q ($r^2 = 0.56$, $p < 0.001$, NSE = 0.56) than in summer ($r^2 = 0.31$, $p < 0.001$, NSE = 0.27), and with moderate concurrence overall ($r^2 = 0.37$, $p < 0.001$, NSE = 0.27) (Table 2). The diel pattern of predicted Q was in sync with observed Q but failed to replicate the bi-modal peaks (Supplementary Figure A8).

At the start of the dry season, with abundant soil moisture conditions in Event 1, the interaction term between S and T (S*T) was a moderately significant ($P = 0.069$) predictor of Q with a negative coefficient, suggesting soil moisture and transpiration are modulating streamflow in combination. As the dry season progressed, T became a more robust predictor of Q during Event 2 ($p = 0.09$) and Event 3 ($p = 0.01$) with negative coefficients and under average S conditions. However, with the advent of precipitation in summer in Event 4, P ($p < 0.001$) was the strongest predictor, followed by M_a ($p = 0.004$). Interestingly, the interactive term S*T remained a predictor of Q with positive coefficients, albeit with lesser significance ($p = 0.12$). Incidentally, T had negative slope coefficients across the dry and wet periods, indicating a loss of potential Q to T.

4. Discussion

The study site is unique in being the wettest high-elevation TMF site in the world (90th percentile of the elevations and 80th percentile of precipitation), where concurrent observations of direct transpiration, streamflow, and micro-climate measurements have been carried out so far (Supplementary Figure A9) (Bruijnzeel et al., 2011; Kumar et al., 2023a; D. McJannet et al., 2007). At the site, the lower latitude (27–28°) and proximity to the south-west Indian monsoon favour tropical climatology, with the bulk of the precipitation occurring in the late-night to early morning period, a phenomenon unique to the

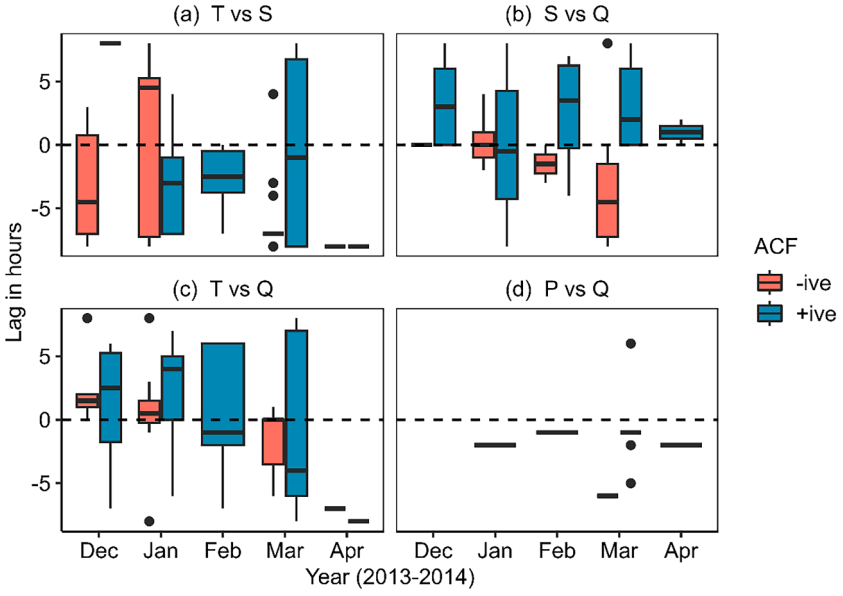

Fig. 6. Boxplots showing diel lag hours at maximum auto-correlation coefficients (ACF) for the combinations: (a) T vs. S, (b) S vs. Q, (c) T vs. Q and (d) P vs. Q.The variables are Stand transpiration (T, mm h^{-1}), Precipitation (P, mm h^{-1}), Soil moisture (, mm) and Streamflow (Q, mm h^{-1}). The horizontal dotted line denotes the zero lag hours.

Table 2
Results from Generalised least squares (GLS) linear regression model with corAR1 correlational structure for streamflow (*$p < 0.05$, ** $p < 0.01$, *** $p < 0.001$). Predictor variables include Stand transpiration (T, mm h^{-1}), Soil moisture (S, mm), Precipitation (P, mm h^{-1}), Antecedent moisture index (M_a, mm h^{-1}), and the response variable is Streamflow (Q, mm h^{-1}). S*T is the interaction term between soil moisture and stand transpiration.

Model	Season	Event (No. of days)	Variables	Lag (L, in h)	Coefficients	Std. Error	t-value	p-value (*p*)
Q ~ S*T	Winter	1 (10 days)	T	0	0.0002	0.0009	0.198	0.84
			S	0	0.0006	0.0007	0.794	0.43
			S* T	0	−0.0186	0.0102	−1.828	0.07
		2 (17 days)	T	0	−0.0011	0.0007	−1.729	0.09
			S	0	−0.0002	0.0005	−0.460	0.65
			S* T	0	−0.0061	0.0055	−1.120	0.26
		3 (6 days)	T	0	−0.0048	0.0019	−2.513	0.01*
			S	0	0.0001	0.0008	0.098	0.92
			S*T	0	−0.0151	0.0146	−1.034	0.30
Q ~ $P + M_a + S$*T	Summer	4 (27 days)	P	1	0.0044	0.0002	24.132	<0.001***
			T	0	−0.0042	0.0042	−0.993	0.32
			S	0	0.0004	0.0008	0.493	0.62
			M_a	0	0.0005	0.0002	2.924	0.004**
			S*T	0	0.0131	0.0084	1.556	0.12

Himalaya (Barros and Lang, 2003). The wet and tropical climatology have supported high transpiration rates in the fast-regenerating secondary forests communities (Kumar et al., 2023a), and this study attempts to understand its impact on hydrological partitioning in data-scarce Eastern Himalaya. The study has two major limitations which hampered catchment water balance estimation: (1) low sample size underlying the sapwood area to tree diameter relationship estimation, which is used for scaling from whole-tree sap flow to stand transpiration, and (2) the inability to monitor soil moisture below 30 cm depth and data gaps due to equipment malfunctions.

Most sap flow studies come from relatively homogenous or well-studied long-term experimental plots and assume a linear fit between tree size and sapwood area for scaling whole-tree sap flow (Asbjornsen et al., 2011; Berry et al., 2018b; Kumagai et al., 2005b). However, the assumptions of linear fit are limited to homogenous stands, and non-linear regression models are recommended for studies in uneven-aged secondary forests (Forrester et al., 2022). While comparing the effect of tree size on scaling from whole-tree sap flow to stand transpiration in South American TMFs, Berry et al. (2018b) stressed on developing an empirical and conceptual understanding of the relationships between tree size, active sapwood and species-specific ecological traits. They highlight that the non-linear increase in sapwood depth with tree diameter in large trees and supply-side constraints on water transport (limitations associated with soil water, stomatal conductance, etc.) can lead to reduced actual water use in large trees than suggested by linear relationships. Thus, despite being limited by 13 instrumented trees in this study, the observed non-linear fit between the sapwood area vs. tree diameter relationship was ecologically appropriate for the secondary forest stand being investigated (Supplementary Figure A3).

Further, field instrumentation in remote, high-elevation Himalayan catchments is challenging, and data losses are a reality. Despite these challenges, the study installed and maintained more than ten different type of environmental sensors that recorded sap flux, soil moisture, streamflow, precipitation, and other micrometeorological variables at high frequency. Due to logistical limitations, we could not monitor the soil moisture at depths greater than 30 cm, which blinds us to any downward moisture flux to the deeper soil layers and contributions to aquifer recharge. We addressed the lacunae through two reasonable and physically sound assumptions: (1) the soil profile acts as a transient storage facilitating moisture transfer between infiltration, evapotranspiration and recharge, and (2) streamflow is inclusive of changes in deep soil moisture and shallow aquifer (D. McJannet et al., 2007). The first assumption is particularly valid for steep mountain catchments like ours with low soil depth and shallow and sloped aquifers (Supplementary Figure A6b) (Fan et al., 2023; Kumar et al., 2023a). It can be assumed that any downward soil moisture flux recharges the aquifer and ultimately contributes to the stream as baseflow. Thus, under non-leaky aquifer conditions, changes in aquifer storage can linearly reflect in streamflow (Q), which supports the second assumption (D. McJannet et al., 2007). However, the assumptions may become invalidated in catchments with deep soils and/or leaky aquifers, and deep soil moisture monitoring and hydrogeological surveys are recommended for future ecohydrological studies in the Himalaya.

4.1. Transpiration in wet TMF of eastern Himalaya

The rate of transpiration in a forest stand provides crucial information regarding the vegetation's capacity to recirculate moisture, which varies considerably with the stand age, species-specific water-use efficiency, and availability of moisture and energy. The observed mean daily transpiration (1.29±0.99 mm d^{-1}) in wetter Eastern Himalaya was found to be approximately double that of the relatively drier Central Himalayan oak forests (MAP = 1331 mm) in Nepal (Ghimire et al., 2014b), but comparable with similarly wet low elevation (450- 650 masl) TMFs (MAP = 4200–5000 mm) in Costa Rica (Aparecido et al., 2016; Moore et al., 2018) and similar elevation TMF (MAP = 2067 mm) in Southern Andes (Motzer et al., 2010). The maximum daily stand transpiration (5.3 mm) is 14% higher than the highest rates (~4.6 mm) reported from tropical montane or lowland forests (Bruijnzeel et al., 2011; D. McJannet et al., 2007). The observed nocturnal transpiration (T_{night}) was similar to studies (~12%) from China (Siddiq and Cao, 2018) and other parts of the globe (Forster, 2014).

Overall, the relatively higher transpiration rates, despite being at a higher elevation, are possibly fueled by faster growth rates and higher interception losses from the secondary forest vegetation in a very wet environment. However, there is a lack of understanding of the changes in functional diversity and forest composition at different successional stages in secondary tropical forests and their impact on carbon and water cycles (Oberleitner et al., 2021; Rozendaal et al., 2021). In the accompanying study, Kumar et al. (2023a) show that the dominant pioneer (*Symplocos racemosa* and *Eurya acuminata*) and late-successional species (*Castanopsis hystrix*) in the studied forest stand have significantly higher sap flux densities than their counterparts in relatively drier parts of Himalaya or in higher latitudes. The high transpiration rates could also indicate their evolution under a relatively wetter climate of Eastern Himalaya and merit further investigations on water-use efficiencies with changing climate (Panthi et al., 2020). Along similar lines, Pandey et al. (2020) have suggested that climate warming and increased summer precipitation will likely remove moisture constraints on photosynthesis on treeline conifer and broad-leaved species in wetter parts of eastern Nepal Himalaya. This is further bolstered by faster transpiration recovery after low-mid-sized precipitation pulses. Such behaviour is accompanied by high evaporative demand (high E_0 and D), as seen in the Australian woodland (Burgess, 2006; Zeppel et al., 2008). It is also

common to forest stands with deep-rooted species (*Castanopsis hystrix*), as seen at the study site (Kumar et al., 2023a) and in the semi-arid parts of China (Chen et al., 2014). Here, the role of low-moderate precipitation pulses after a prolonged dry period becomes crucial for the shallow-rooted pioneer species and less for the deep-rooted late--successional species. Thus, with climate change, the predicted decline in winter precipitation and small precipitation events may significantly impact the species composition and primary productivity of these regenerating secondary forests (Krishnan et al., 2019; Krishnaswamy et al., 2014).

4.2. Role of transpiration in catchment ecohydrology

In wet secondary TMFs with high transpiration rates, stand transpiration and canopy interception losses can exceed reference evapotranspiration estimated using micro-meteorological data (Kumar et al., 2023a). Thus, studies lacking direct measurements of transpiration and interception losses can underestimate the contribution of total evapotranspiration to water balance. This gap in our understanding of water balance in high-altitude TMFs is further accentuated by steep gradients and heterogenous canopy, which reduce the accuracy of remotely-sensed evapotranspiration (Núñez et al., 2021). Our inability to monitor deep soil moisture flux may confound the overestimation of E_{loss}, although high fractions of evapotranspiration to precipitation are common in wet regions of the globe (Ukkola and Prentice, 2013). Similar to our study, Leopoldo et al. (1995) used direct sap flow methods to show evapotranspiration constituting up to two-thirds of the annual water balance in a forested catchment in Brazil, including 57% contribution of transpiration. D. McJannet et al. (2007) reported high fractions (13–50%) of T and other evaporative losses to annual precipitation using direct sap flow methods in mountain forests of Australia. Other studies have estimated traditional evapotranspiration estimates using microclimatic data to report high fractions of E_0 to annual P (68%) in high Andean mountains (Rodríguez-Morales et al., 2019) in a subalpine catchment in China (69–94%) (Yan et al., 2017), and in neighbouring Bhutan (mean±SD, 46±6%) (Dorji et al., 2016). However, the fraction of T to total evapotranspiration losses (5–15%) estimated through catchment water balance was similar to the results from mixed-oak forests (14%) in drier Central Himalaya (Ghimire et al., 2014b).

Few studies have explored the interactions between vegetation water use, soil moisture, and streamflow at a fine temporal resolution in TMFs (Ghimire et al., 2014b; Kumar et al., 2023a; Rai and Sharma, 1998). Interestingly, the catchment water balance was first modulated by soil moisture, and after its saturation, evapotranspiration and streamflow components increased in significance. The results, along with the changes from bimodal to unimodal peaks in diel streamflow, illustrate mechanistic linkages between T, S and Q after a precipitation event and over changing antecedent moisture conditions (Hou et al., 2023). As observed at the study site, low soil infiltration rates and high precipitation intensities may lead to high infiltration-excess runoff generation in the wet season (Ghimire et al., 2014a; Nanda et al., 2019). Conversely, high moisture uptake by vegetation may lead to relatively lower streamflow output in the dry season compared to a primary forest (Wright et al., 2018). The phase lags between T, S and Q were confounded by significant pre-dawn sap flux movement (Kumar et al., 2023a) and the presence of secondary diel peaks in S and Q. The catchment response to precipitation pulses varied with antecedent moisture conditions, and the corresponding increase in T after medium-large pulses had a stronger negative influence on S and Q than after small precipitation events. An experimental study with orange trees reported similar patterns of mid-sized precipitation (>10 mm) leading to an increase in transpiration on subsequent days, while low precipitation pulses had a negative effect (Hou et al., 2023). It is likely that moderate-sized precipitation pulses, after a prolonged dry period, replenish the soil moisture stock, while boosting T, whereas small precipitation pulses provide little contribution to S and Q but trigger high T responses, thereby inducing the negative effect. Future research could combine using isotope-based methods with sap flow studies to shed better light on these complex interactions. At a coarser scale, Chanda et al. (2024) show that the positive impact of precipitation on forest productivity (measured as NDVI) is visible at a lag of 2-3 months in the Eastern Himalaya. The GLS model results also showed that transpiration exerted significant controls on the diel and seasonal streamflow, with soil moisture acting as the mediator in winter. Similar to evidence from headwater catchments in the USA and the UK, T and its interaction term with S were significant predictors of Q with significant negative coefficients, indicating that high T leads to a decline in Q (Bond et al., 2002; Thomas et al., 2012). Coupled with evidence that Himalayan tree species can extend roots up to 150 cm (Pathak et al., 2021), at the study site, Kumar et al. (2023a) observed that the deep-rooted Fagaceae species *Castanopsis Hystrix* can access deeper moisture layers, which otherwise would have contributed to the stream as baseflow. In the summers, precipitation and antecedent moisture (M_a) were the principal drivers of streamflow. However, the interaction term between T and S remained a significant predictor, signalling continued water uptake by vegetation.

The observed bimodal peaks in Q_{diel} during precipitation-free days are more common in catchments with multiple hydrological controls, i.e., hydrogeological and evapotranspiration (la Cecilia and Camporese, 2022; McMillan, 2020). The observed morning maxima in streamflow are commonly attributed to evapotranspiration (Graham et al., 2013; McMillan, 2020; Moore et al., 2011), while the sharp decline and slow recovery (Supplementary Figure A5) indicate variability in baseflow and interflow contributions to the streamflow (Lundquist and Cayan, 2002; McMillan, 2020). As a fraction of Q, the diel fluctuations were at the higher end of observations from small catchments in the USA (Gannon et al., 2020) and exceeded the 30% significance threshold suggested by Lundquist and Cayan (2002) on at least one-fifth of the total days. The significance threshold is a function of catchment size, gradient and variability in stream velocities across different seasons and, thus, is likely to be lower for headwater catchments than low-elevation floodplains (Wondzell et al., 2007). The amplitude-to-discharge fraction appears to be a function of the evapotranspiration demand, the extent to which sub-surface moisture is available for transpiration and/or evaporation, and the magnitude of the total discharge, all of which are highest in the summer and lowest in the winter (Lundquist and Cayan, 2002; McMillan, 2020). Thus, the diel cycles in streamflow gained significance with the progression of dry periods and synchronised increase in vegetation activity, highlighting the controls exerted by evapotranspiration on streamflow (Bond et al., 2002; Moore et al., 2011). The increasing amplitudes of diel streamflow from winters to summers signified the growing abstraction by vegetation to support primary productivity in the dry season (Barbeta and Peñuelas, 2017; Lundquist and Cayan, 2002). Referring back to the literature on the isotopic separation of water that contributes to transpiration and streamflow (Barbeta and Peñuelas, 2017; Berry et al., 2018a), we suggest that in these broad-leaved Himalayan TMFs with steep slopes and shallow soils, trees can access deeper sub-surface water for transpiration. Evidence of this is shown by Kumar et al. (2023a) at the study site, where groundwater is well within reach of deep-rooted tree species like *C. hystrix,* allowing them to continue transpiring at the peak of the dry season, while shallow-rooted fast-growing pioneer species like *S. racemosa* and *E. acuminata* propelled vegetation water use in moisture abundant conditions in summer.

Thus, in a regenerating secondary forest, stand transpiration can have a significant impact on streamflow (Wright et al., 2018). Studies on climate change in the Eastern Himalaya have predicted an increase in summer precipitation, declining winter precipitation, and increasing summer and winter temperatures (Krishnan et al., 2019; Kumar et al., 2021). In summer, precipitation provides enough moisture to ensure peak vegetation productivity in April. At the site, the summer precipitation predominantly falls in the afternoon period, which, coupled with

evidence of the pre-dawn onset of sap flow in both pioneer and late-successional species, suggests considerable plasticity in the ecophysiological traits related to plant-water use in a wet and tropical montane environment (Kangur et al., 2021; Kumar et al., 2023a). However, increased summer precipitation in future could result in higher cloud cover, negatively impacting both vegetation productivity and transpiration, leading to increased streamflow (Donohue et al., 2017). The overall effect of temperature and precipitation changes on biodiversity in the region remains complex and requires ecohydrological models specific to the East Himalayan TMFs (Asbjornsen et al., 2011).

5. Conclusions

Globally, the effect of vegetation water-use on streamflow varies greatly due to species-specific, environmental and geomorphological peculiarities (Asbjornsen et al., 2011; Wright et al., 2018). High moisture availability, tropical climatology, and regenerating secondary forests provide unique conditions for observing plant-water relations and hydrological services, hitherto unstudied in the Himalaya (Kumar et al., 2023a). These are the first empirical observations of mechanistic control of transpiration on streamflow from the Himalaya and add to the observations drawn by previous studies in the region and to the literature on wet TMFs globally. Stand transpiration is double that of relatively drier Central Himalaya (Ghimire et al., 2014b) but at the lower bound of the values reported from tropical montane cloud forests globally (Bruijnzeel et al., 2011). It indicates the interactive role of precipitation and elevation in modulating the available energy and moisture, which in turn modulates the plant productivity and transpiration rates in fast-regenerating secondary TMFs. Transpiration and other evaporative losses formed a significant part of the catchment water balance. Transpiration was a significant predictor of streamflow in the dry season and, to a lesser extent, in the wet season. The study shows that moderate precipitation pulses followed by clear skies can significantly increase stand transpiration. Thus, changes in vegetation cover and precipitation patterns with climate change may significantly impact the vegetation-streamflow linkages in the secondary broad-leaved tropical montane forests in the Eastern Himalaya. The studied broad-leaved montane forests in Eastern Himalaya are the most species-rich in the world and have experienced considerable human pressures (Kanade and John, 2018; Sudhakar et al., 2008). The TMFs provide protective catchments for the principal water resources, the springs, and streams, and thus, better understanding their plant-soil-streamflow processes is critical to quantifying the ecosystem services, addressing regional water security issues (Kumar et al., 2023b) and ecosystem modelling efforts (Krishnaswamy et al., 2014; Sebastian et al., 2019). We suggest that including diel and seasonal variability in stand transpiration will be critical to increasing the accuracy of land-surface interaction models, and predicting the impact of climate change on Himalayan ecohydrology.

Funding support

The study was funded by the Department of Biotechnology, Govt. of India (GoI) as part of the research project titled “Technological Innovations and Ecological Research for the Sustainable Use of Bioresources in the Eastern Himalaya” (Grant No. BT/01/NE/PS/NCBS/09). The authors are also grateful to the fellowship support provided by the National Mission for Himalayan Studies (NMHS) under the Ministry of Environment, Forest and Climate Change, GoI for further fellowship support during the writing period (Grant No: GBPI/NMHS/HF/RA/2015–16/).

Data sharing

The data supporting the findings of this study are available from the corresponding author, Manish Kumar, on request. A sample subset of the data supporting the findings of this study is also available in the Dryad Digital Repository at https://datadryad.org/stash/share/bkDWLqnM4S2C3w0wgri1AcXlyDz3eM2Sgs7prOqLZqk.

CRediT authorship contribution statement

Manish Kumar: Conceptualization, Data curation, Formal analysis, Investigation, Methodology, Project administration, Software, Validation, Visualization, Writing – original draft, Writing – review & editing. **Yangchenla Bhutia:** Data curation, Formal analysis, Writing – review & editing. **Girish R Varma:** Data curation, Formal analysis, Writing – review & editing. **Gladwin Joseph:** Conceptualization, Formal analysis, Methodology, Resources, Supervision, Writing – review & editing. **Jagdish Krishnaswamy:** Conceptualization, Formal analysis, Funding acquisition, Methodology, Resources, Supervision, Writing – review & editing.

Declaration of competing interest

The authors declare that they have no known competing financial interests or personal relationships that could have appeared to influence the work reported in this paper.

Acknowledgments

The authors are thankful to the Manipal Academy of Higher Education (MAHE), Manipal, India for institutional support. The authors thank the Department of Forests, Environment and Wildlife Management, Rural Management and Development Department, Home Department, Govt. of Sikkim, India, and the Indian Army for research permits and field support. The study would not have been possible without the able field support from Passang Tamang, Naresh Rai, and the staff of Fambong-Loh Wildlife Sanctuary. We thank Mr Mayank Singh for designing the graphical abstract. The authors thank Dr Sumit Sen, Dr Nachiket Kelkar, and Dr Aniruddha Marathe for their valuable comments on hydrological and statistical analysis, and Mr Lalit Kumar Rai and Dr Radhika Kanade for their valuable insights on forest ecology. The authors are indebted to Prof. Nathan G. Phillips at Boston University, USA, Prof. Frederick Meinzer at Oregon State University, USA, and Forests Science Laboratory (Corvallis), USA, for generously sharing the original thermal dissipation probe assembly design. The authors acknowledge the logistical support provided by the ATREE Regional Office, Gangtok, and the National Center for Biological Sciences, Bangalore, India.

Supplementary materials

Supplementary material associated with this article can be found, in the online version, at doi:10.1016/j.ecohyd.2024.04.001.

References

Allen, R.G., Pereira, L.S., Raes, D., Smith, M., 1998. Crop evapotranspiration: guidelines for computing crop requirements. Irrig. Drain. Pap. No. 56 https://doi.org/10.1016/j.eja.2010.12.001. FAO 300.

Aparecido, L.M.T., Miller, G.R., Cahill, A.T., Moore, G.W., 2016. Comparison of tree transpiration under wet and dry canopy conditions in a Costa Rican premontane tropical forest. Hydrol. Process. 30, 5000–5011. https://doi.org/10.1002/hyp.10960.

Asbjornsen, H., Goldsmith, G.R., Alvarado-Barrientos, M.S., Rebel, K., Van Osch, F.P., Rietkerk, M., Chen, J., Gotsch, S., Tobón, C., Geissert, D.R., Gómez-Tagle, A., Vache, K., Dawson, T.E., 2011. Ecohydrological advances and applications in plant-water relations research: a review. J. Plant Ecol. https://doi.org/10.1093/jpe/rtr005.

Badu, M., Ghimire, C.P., Bruijnzeel, L.A., Nuberg, I., Meyer, W.S., 2022. Net precipitation, infiltration and overland flow production in three types of community-managed forest in the Mid-hills of East Central Nepal. Trees, For. People, 100218. https://doi.org/10.1016/j.tfp.2022.100218.

Barbeta, A., Peñuelas, J., 2017. Relative contribution of groundwater to plant transpiration estimated with stable isotopes. Sci. Rep. 7, 1–10. https://doi.org/10.1038/s41598-017-09643-x.

Barros, A.P., Lang, T.J., 2003. Monitoring the monsoon in the himalayas: observations in central Nepal, June 2001. Mon. Weather Rev. 131, 1408–1427. https://doi.org/10.1175/1520-0493(2003)131. <1408:MTMITH>2.0.CO;2.

Berry, Z.C., Evaristo, J., Moore, G., Poca, M., Steppe, K., Verrot, L., Asbjornsen, H., Borma, L.S., Bretfeld, M., Hervé-Fernández, P., Seyfried, M., Schwendenmann, L., Sinacore, K., De Wispelaere, L., McDonnell, J., 2018a. The two water worlds hypothesis: addressing multiple working hypotheses and proposing a way forward. Ecohydrology 11. https://doi.org/10.1002/eco.1843.

Berry, Z.C., Looker, N., Holwerda, F., Gómez Aguilar, L.R., Ortiz Colin, P., González Martínez, T., Asbjornsen, H., 2018b. Why size matters: the interactive influences of tree diameter distribution and sap flow parameters on upscaled transpiration. Tree Physiol 38, 264–276. https://doi.org/10.1093/treephys/tpx124.

Bhutia, Y., Gudasalamani, R., Ganesan, R., Saha, S., 2019. Assessing forest structure and composition along the altitudinal gradient in the state of Sikkim. Eastern Himalayas, India. Forests 10, 1–17. https://doi.org/10.3390/f10080633.

Bond, B.J., Jones, J.a., Moore, G., Phillips, N., Post, D., McDonnell, J.J., 2002. The zone of vegetation influence on baseflow revealed by diel patterns of streamflow and vegetation water use in a headwater basin. Hydrol. Process. 16, 1671–1677. https://doi.org/10.1002/hyp.5022.

Bonnesoeur, V., Locatelli, B., Guariguata, M.R., Ochoa-Tocachi, B.F., Vanacker, V., Mao, Z., Stokes, A., Mathez-Stiefel, S.L., 2019. Impacts of forests and forestation on hydrological services in the Andes: a systematic review. For. Ecol. Manage. 433, 569–584. https://doi.org/10.1016/j.foreco.2018.11.033.

Bouyoucos, G.J., 1928. The hydrometer method for studying soils. Soil Sci. https://doi.org/10.1097/00010694-192805000-00007.

Bruijnzeel, L.A., Mulligan, M., Scatena, F.N., 2011. Hydrometeorology of tropical montane cloud forests: emerging patterns. Hydrol. Process. 25, 465–498. https://doi.org/10.1002/hyp.7974.

Burgess, S.S.O., 2006. Measuring transpiration responses to summer precipitation in a Mediterranean climate: a simple screening tool for identifying plant water-use strategies. Physiol. Plant. 127, 404–412. https://doi.org/10.1111/j.1399-3054.2006.00669.x.

Célleri, R., Feyen, J., 2009. The Hydrology of Tropical Andean Ecosystems: importance, Knowledge Status, and Perspectives. Mt. Res. Dev. 29, 350–355. https://doi.org/10.1659/mrd.00007.

Chanda, R., Singh, S.S., Singh, N.S., Upadhyay, K.K., Tripathi, S.K., 2024. Two-decadal climate impacts on growth of major forest types of Eastern Himalaya. Trees For. People 15, 100491.

Chen, L., Zhang, Z., Zeppel, M., Liu, C., Guo, J., Zhu, J., Zhang, X., Zhang, J., Zha, T., 2014. Response of transpiration to rain pulses for two tree species in a semiarid plantation. Int. J. Biometeorol. 58, 1569–1581. https://doi.org/10.1007/s00484-013-0761-9.

Chiariello, N.R., Field, C.B., Mooney, H.A., 2006. Midday wilting in a tropical pioneer tree. Funct. Ecol. 1, 3–11.

Chiu, C.W., Komatsu, H., Katayama, A., Otsuki, K., 2016. Scaling-up from tree to stand transpiration for a warm-temperate multi-specific broadleaved forest with a wide variation in stem diameter. J. For. Res. 21, 161–169. https://doi.org/10.1007/s10310-016-0532-7.

Davis, T.W., Kuo, C.-M., Liang, X., Yu, P.-S., 2012. Sap flow sensors: construction, quality control and comparison. Sensors (Basel) 12, 954–971. https://doi.org/10.3390/s120100954.

Deng, Y., Wu, S., Ke, J., Zhu, A., 2021. Effects of meteorological factors and groundwater depths on plant sap flow velocities in karst critical zone. Sci. Total Environ. 781, 146764 https://doi.org/10.1016/j.scitotenv.2021.146764.

Dib, V., Brancalion, P.H.S., Chan Chou, S., Cooper, M., Ellison, D., Farjalla, V.F., Filoso, S., Meli, P., Pires, A.P.F., Rodriguez, D.A., Iribarrem, A., Latawiec, A.E., Scarano, F.R., Vogl, A.L., de Viveiros Grelle, C.E., Strassburg, B., 2023. Shedding light on the complex relationship between forest restoration and water services. Restor. Ecol. 31, 1–6. https://doi.org/10.1111/rec.13890.

Donohue, R.J., Roderick, M.L., McVicar, T.R., Yang, Y., 2017. A simple hypothesis of how leaf and canopy-level transpiration and assimilation respond to elevated CO2 reveals distinct response patterns between disturbed and undisturbed vegetation. J. Geophys. Res. Biogeosciences 122, 168–184. https://doi.org/10.1002/2016JG003505.

Dorji, U., Olesen, J.E., Seidenkrantz, M.S., 2016. Water balance in the complex mountainous terrain of Bhutan and linkages to land use. J. Hydrol. Reg. Stud. 7, 55–68. https://doi.org/10.1016/j.ejrh.2016.05.001.

Evaristo, J., Jasechko, S., McDonnell, J.J., 2015. Global separation of plant transpiration from groundwater and streamflow. Nature 525, 91–94. https://doi.org/10.1038/nature14983.

Fan, L., Kuang, X., Or, D., Zheng, C., 2023. Streamflow composition and water "imbalance" in the Northern Himalayas. Water Resour. Res. 59, 1–19. https://doi.org/10.1029/2022WR034243.

Flo, V., Martinez-Vilalta, J., Steppe, K., Schuldt, B., Poyatos, R., 2019. A synthesis of bias and uncertainty in sap flow methods. Agric. For. Meteorol. 271, 362–374. https://doi.org/10.1016/j.agrformet.2019.03.012.

Forrester, D.I., Limousin, J.M., Pfautsch, S., 2022. The relationship between tree size and tree water-use: is competition for water size-symmetric or size-asymmetric? Tree Physiol 42, 1916–1927. https://doi.org/10.1093/treephys/tpac018.

Forster, M.A., 2014. How significant is nocturnal sap flow? Tree Physiol. 34, 757–765. https://doi.org/10.1093/treephys/tpu051.

Franco, A.C., Lüttge, U., 2002. Midday depression in savanna trees: coordinatedadjustments in photochemical effiiency, photorespiration, CO_2 assimilation andwater use effiiency. Oecologia 131, 356–365.

Gannon, J.P., Kinner, D., Styers, D., Lord, M., 2020. Diel discharge variations in dormant and growing seasons in a headwater catchment suggest potential sources of an evapotranspiration signal. Hydrol. Process. 34, 1228–1236. https://doi.org/10.1002/hyp.13670.

Ghimire, C.P., Bruijnzeel, L.A., Bonell, M., Coles, N., Lubczynski, M.W., Gilmour, D.A., 2014a. The effects of sustained forest use on hillslope soil hydraulic conductivity in the Middle Mountains of Central Nepal. Ecohydrology 7, 478–495. https://doi.org/10.1002/eco.1367.

Ghimire, C.P., Lubczynski, M.W., Bruijnzeel, L.A., Chavarro-Rincón, D., 2014b. Transpiration and canopy conductance of two contrasting forest types in the Lesser Himalaya of Central Nepal. Agric. For. Meteorol. 197, 76–90. https://doi.org/10.1016/j.agrformet.2014.05.012.

Graham, C.B., Barnard, H.R., Kavanagh, K.L., Mcnamara, J.P., 2013. Catchment scale controls the temporal connection of transpiration and diel fluctuations in streamflow. Hydrol. Process. 27, 2541–2556. https://doi.org/10.1002/hyp.9334.

Granier, A., 1987. Evaluation of transpiration in a Douglas-fir stand by means of sap flow measurements. Tree Physiol. 3, 309–320.

Gribovszki, Z., Szilágyi, J., Kalicz, P., 2010. Diurnal fluctuations in shallow groundwater levels and streamflow rates and their interpretation - A review. J. Hydrol. 385, 371–383. https://doi.org/10.1016/j.jhydrol.2010.02.001.

Gupta, H.V., Kling, H., 2011. On typical range, sensitivity, and normalization of Mean Squared Error and Nash-Sutcliffe Efficiency type metrics. Water Resour. Res. 47, 2–4. https://doi.org/10.1029/2011WR010962.

Heinrich, V.H.A., Vancutsem, C., Dalagnol, R., Rosan, T.M., Fawcett, D., Silva-Junior, C. H.L., Cassol, H.L.G., Achard, F., Jucker, T., Silva, C.A., House, J., Sitch, S., Hales, T. C., Aragão, L.E.O.C., 2023. The carbon sink of secondary and degraded humid tropical forests. Nature 615, 436–442. https://doi.org/10.1038/s41586-022-05679-w.

Hou, P., Chen, D., Wei, X., Hu, X., Duan, X., Zhang, J., Qiu, L., Zhang, L., 2023. Transpiration characteristics and environmental controls of orange orchards in the dry-hot valley region of southwest China. Agric. Water Manag. 288, 108467 https://doi.org/10.1016/j.agwat.2023.108467.

Jasechko, S., Sharp, Z.D., Gibson, J.J., Birks, S.J., Yi, Y., Fawcett, P.J., 2013. Terrestrial water fluxes dominated by transpiration. Nature 496, 347–350. https://doi.org/10.1038/nature11983.

Kanade, R., John, R., 2018. Topographical influence on recent deforestation and degradation in the Sikkim Himalaya in India; Implications for conservation of East Himalayan broadleaf forest. Appl. Geogr. 92, 85–93. https://doi.org/10.1016/j.apgeog.2018.02.004.

Kangur, O., Steppe, K., Schreel, J.D.M., Von Der Crone, J.S., Sellin, A., 2021. Variation in nocturnal stomatal conductance and development of predawn disequilibrium between soil and leaf water potentials in nine temperate deciduous tree species. Funct. Plant Biol. 48, 483–492. https://doi.org/10.1071/FP20091.

Kirchner, J.W., Godsey, S.E., Solomon, M., Osterhuber, R., McConnell, J.R., Penna, D., 2020. The pulse of a montane ecosystem: coupling between daily cycles in solar flux, snowmelt, transpiration, groundwater, and streamflow at Sagehen Creek and Independence Creek, Sierra Nevada, USA. Hydrol. Earth Syst. Sci. 24, 5095–5123. https://doi.org/10.5194/hess-24-5095-2020.

Krishnan, R., Shrestha, Arun B, Ren, G., Rajbhandari, R., Saeed, S., Sanjay, J., Syed, A., Vellore, R., Xu, Y., You, Q., Ren, Y., 2019. Unravelling climate change in the hindu kush himalaya: rapid warming in the mountains and increasing extremes. In: Wester, P., Mishra, A., Mukherji, A., Shrestha, Arun Bhakta, Change, C. (Eds.), The Hindu Kush Himalaya Assessment. Springer International Publishing. https://doi.org/10.1007/978-3-319-92288-1.

Krishnaswamy, J., García Chevesich, P., Neary, D.G., Scott, D.F., Benyon, R.G., 2017. Forest management and water in India. In: Reyna, T. (Ed.), Forest Management and the Impact on Water Resources: A Review of 13 Countries. UNESCO Publishing, pp. 87–104.

Krishnaswamy, J., Bonell, M., Venkatesh, B., Purandara, B.K., Lele, S., Kiran, M.C., Reddy, V., Badiger, S., Rakesh, K.N., 2012. The rain-runoff response of tropical humid forest ecosystems to use and reforestation in the western ghats of India. J. Hydrol. 472-473, 216–237. https://doi.org/10.1016/j.jhydrol.2012.09.016.

Krishnaswamy, J., John, R., Joseph, S., 2014. Consistent response of vegetation dynamics to recent climate change in tropical mountain regions. Glob. Chang. Biol. 20, 203–215. https://doi.org/10.1111/gcb.12362.

Kumagai, T., Aoki, S., Nagasawa, H., Mabuchi, T., Kubota, K., Inoue, S., Utsumi, Y., Otsuki, K., 2005a. Effects of tree-to-tree and radial variations on sap flow estimates of transpiration in Japanese cedar. Agric. For. Meteorol. 135, 110–116. https://doi.org/10.1016/j.agrformet.2005.11.007.

Kumagai, T., Nagasawa, H., Mabuchi, T., Ohsaki, S., Kubota, K., Kogi, K., Utsumi, Y., Koga, S., Otsuki, K., 2005b. Sources of error in estimating stand transpiration using allometric relationships between stem diameter and sapwood area for Cryptomeria japonica and Chamaecyparis obtusa. For. Ecol. Manage. 206, 191–195. https://doi.org/10.1016/j.foreco.2004.10.066.

Kumar, M., Hodnebrog, Ø., Sophie Daloz, A., Sen, S., Badiger, S., Krishnaswamy, J., 2021. Measuring precipitation in Eastern Himalaya: ground validation of eleven satellite, model and gauge interpolated gridded products. J. Hydrol. 599 https://doi.org/10.1016/j.jhydrol.2021.126252.

Kumar, M., Joseph, G., Bhutia, Y., 2023a. Contrasting sap flow characteristics between pioneer and late-successional tree species in secondary tropical montane forests of Eastern Himalaya. India. J. Exp. Bot. https://doi.org/10.1093/jxb/erad207.

Kumar, M., Rathod, R., Mukherji, A., 2023b. Water security and spring conservation in the Himalaya. In: Ojha, H., Schofield, N., Camkin, J. (Eds.), Climate Risks to Water

Security: Framing Effective Response in Asia and the Pacific. Palgrave Macmillan, Singapore, pp. 1–21.
la Cecilia, D., Camporese, M., 2022. Resolving streamflow diel fluctuations in a small agricultural catchment with an integrated surface-subsurface hydrological model. Hydrol. Process. 36, 1–15. https://doi.org/10.1002/hyp.14768.
Larson, P., Runyan, C., 2009. Evaluation of a capacitance water level recorder and calibration methods in an Urban Environment. CUERE Tech. Memo 36.
Lehnebach, R., Morel, H., Bossu, J., Le Moguédec, G., Amusant, N., Beauchêne, J., Nicolini, E., 2017. Heartwood/sapwood profile and the tradeoff between trunk and crown increment in a natural forest: the case study of a tropical tree (Dicorynia guianensis Amsh., Fabaceae). Trees - Struct. Funct. 31, 199–214. https://doi.org/10.1007/s00468-016-1473-7.
Leopoldo, P.R., Franken, W.K., Villa Nova, N.A., 1995. Real evapotranspiration and transpiration through a tropical rain forest in central Amazonia as estimated by the water balance method. For. Ecol. Manage. 73, 185–195. https://doi.org/10.1016/0378-1127(94)03487-H.
Li, S., Xu, Z., Yu, Z., Fu, Y., Su, X., Zou, B., Wang, S., Huang, Z., Wan, X., 2023. Litter decomposition and nutrient release are faster under secondary forests than under Chinese fir plantations with forest development. Sci. Rep. 13, 1–10. https://doi.org/10.1038/s41598-023-44042-5.
Lu, P., Urban, L., Ping, Z., 2004. Granier ' s thermal dissipation probe (TDP) method for measuring sap flow in trees : theory and practice 1 granier sap flow measuring method : acta bot. Sin. 46, 631–646, 316-646.
Lundquist, J.D., Cayan, D.R., 2002. Seasonal and spatial patterns in diurnal cycles in streamflow in the western United States. J. Hydrometeorol. 3, 591–603. https://doi.org/10.1175/1525-7541(2002)003<0591:SASPID>2.0.CO;2.
Mackay, D.S., Ewers, B.E., Loranty, M.M., Kruger, E.L., 2010. On the representativeness of plot size and location for scaling transpiration from trees to a stand. J. Geophys. Res. 115, G02016. https://doi.org/10.1029/2009JG001092.
Maeght, J., Rewald, B., Pierret, A., 2013. How to study deep roots—and why it matters. Front. Plant Sci. 4, 1–14. https://doi.org/10.3389/fpls.2013.00299.
McJannet, D., Fitch, P., Disher, M., Wallace, J., 2007a. Measurements of transpiration in four tropical rainforest types of north Queensland. Australia. Hydrol. Process. 21, 3549–3564. https://doi.org/10.1002/hyp.
McJannet, D., Wallace, J., Fitch, P., Disher, M., Reddell, P., 2007b. Water balance of tropical rainforest canopies in northQueensland. Australia. Hydrol. Process. 21, 3473–3484. https://doi.org/10.1002/hyp.
McMillan, H., 2020. Linking hydrologic signatures to hydrologic processes: a review. Hydrol. Process. 34, 1393–1409. https://doi.org/10.1002/hyp.13632.
Moore, G.W., Jones, J.A., Bond, B.J., 2011. How soil moisture mediates the influence of transpiration on streamflow at hourly to interannual scales in a forested catchment. Hydrol. Process. 25, 3701–3710. https://doi.org/10.1002/hyp.8095.
Moore, G.W., Orozco, G., Aparecido, L.M.T., Miller, G.R., 2018. Upscaling transpiration in diverse forests: insights from a tropical premontane site. Ecohydrology 11, 1–13. https://doi.org/10.1002/eco.1920.
Motzer, T., Munz, N., Anhuf, D., Küppers, M., 2010. Transpiration and microclimate of a tropical montane rain forest, southern Ecuador. H.L.S.. In: Bruijnzeel, L.A., Scatena, F.N. (Eds.), Tropical Montane Cloud Forests: Science for Conservation and Management. Cambridge University Press, pp. 447–455. https://doi.org/10.1017/CBO9780511778384.049.
Myneni, R., Knyazikhin, Y., Park, T., 2015. MOD15A2H modis leaf area index/FPAR 8-Day L4 Global 500m SIN Grid V006, DAAC. NASA EOSDIS Land Processes. https://doi.org/10.5067/MODIS/MOD15A2H.006. Terra.
Nachabe, M., Shah, N., Ross, M., Vomacka, J., 2005. Evapotranspiration of two vegetation covers in a shallow water table environment. Soil Sci. Soc. Am. J. 69, 492. https://doi.org/10.2136/sssaj2005.0492.
Nanda, A., Sen, S., Mcnamara, J.P., 2019. How spatiotemporal variation of soil moisture can explain hydrological connectivity of in fi ltration-excess dominated hillslope : observations from lesser Himalayan landscape. J. Hydrol. 124146 https://doi.org/10.1016/j.jhydrol.2019.124146.
Nayak, R.R., Krishnaswamy, J., Vaidyanathan, S., Chappell, N.A., Bhalla, R.S., 2023. Invasion of natural grasslands by exotic trees increases flood risks in mountainous landscapes in South India. J. Hydrol. 617, 128944 https://doi.org/10.1016/j.jhydrol.2022.128944.
Núñez, P.Á., Silva, B., Schulz, M., Rollenbeck, R., Bendix, J., 2021. Evapotranspiration estimates for two tropical mountain forest using high spatial resolution satellite data. Int. J. Remote Sens. 42, 2940–2962. https://doi.org/10.1080/01431161.2020.1864058.
Oberleitner, F., Egger, C., Oberdorfer, S., Dullinger, S., Wanek, W., Hietz, P., 2021. Recovery of aboveground biomass, species richness and composition in tropical secondary forests in SW Costa Rica. For. Ecol. Manage. 479, 118580 https://doi.org/10.1016/j.foreco.2020.118580.
Pandey, P.K., Dabral, P.P., Pandey, V., 2016. Evaluation of reference evapotranspiration methods for the northeastern region of India. Int. Soil Water Conserv. Res. 4, 52–63. https://doi.org/10.1016/j.iswcr.2016.02.003.
Pandey, R., Rawat, M., Singh, R., Bala, N., 2023. Large scale spatial assessment, modelling and identification of drivers of soil respiration in the Western Himalayan temperate forest. Ecol. Indic. 146, 109927 https://doi.org/10.1016/j.ecolind.2023.109927.
Pandey, S., Cherubini, P., Saurer, M., Carrer, M., Petit, G., 2020. Effects of climate change on treeline trees in Sagarmatha (Mt. Everest, Central Himalaya). J. Veg. Sci. 31, 1146–1155. https://doi.org/10.1111/jvs.12921.
Panthi, S., Fan, Z.X., van der Sleen, P., Zuidema, P.A., 2020. Long-term physiological and growth responses of Himalayan fir to environmental change are mediated by mean climate. Glob. Chang. Biol. 26, 1778–1794. https://doi.org/10.1111/gcb.14910.
Pathak, G.C., Joshi, H., Singh, R.D., Tewari, A., Pandey, R., Singh, S.P., 2021. Vertical root distribution in Himalayan trees: about half of roots occur below 30cm, the generally sampled depth. Trop. Ecol. 62, 479–491. https://doi.org/10.1007/s42965-021-00159-0.
Peña-Arancibia, J.L., Bruijnzeel, L.A., Mulligan, M., van Dijk, A.I.J.M., 2019. Forests as 'sponges' and 'pumps': assessing the impact of deforestation on dry-season flows across the tropics. J. Hydrol. 574, 946–963. https://doi.org/10.1016/j.jhydrol.2019.04.064.
Perry, T.D., Jones, J.A., 2017. Summer streamflow deficits from regenerating Douglas-fir forest in the Pacific Northwest. USA. Ecohydrology 10, 1–13. https://doi.org/10.1002/eco.1790.
Pinheiro, J., Bates, D., 2006. *Mixed-effects models in S and S-PLUS*. Springer Science & Business Media.
Potts, D.L., Huxman, T.E., Cable, J.M., English, N.B., Ignace, D.D., Eilts, J.A., Mason, M. J., Weltzin, J.F., Williams, D.G., 2006. Antecedent moisture and seasonal precipitation influence the response of canopy-scale carbon and water exchange to rainfall pulses in a semi-arid grassland. New Phytol 170, 849–860. https://doi.org/10.1111/j.1469-8137.2006.01732.x.
Qazi, N.Q., Bruijnzeel, L.A., Rai, S.P., Ghimire, C.P., 2017. Impact of forest degradation on streamflow regime and runoff response to rainfall in the Garhwal Himalaya. Northwest India. Hydrol. Sci. J. 62, 1114–1130. https://doi.org/10.1080/02626667.2017.1308637.
R Core Team, 2024. R: A language and Environment For Statistical computing. R Foundation For Statistical Computing. Vienna, Austria. https://doi.org/10.1108/eb003648.
Rai, S.C., Sharma, E., 1998. Comparative assessment of runoff characteristics under different land use patterns within a Himalayan watershed. Hydrol. Process. 12, 2235–2248. https://doi.org/10.1002/(sici)1099-1085(19981030)12:13/14<2235::aid-hyp732>3.0.co;2-5.
Ramakrishnan, P.S., Kushwaha, S.P.S., 2001. Secondary forests of the Himalaya with emphasis on the north-eastern hill region of India. J. Trop. For. Sci. 727–747.
Rodríguez-Morales, M., Acevedo-Novoa, D., Machado, D., Ablan, M., Dugarte, W., Dávila, F., 2019. Ecohydrology of the Venezuelan páramo: water balance of a high Andean watershed. Plant Ecol. Divers. 12, 573–591. https://doi.org/10.1080/17550874.2019.1673494.
Rozendaal, M.A., Bongers, F., Almeida, D.J.S., Alvarez, F.S., Mart, M., Mora, F., Moreno, V.D.S., Sandra, C.M., Mu, R., Meave, J.A., Muscarella, R., Nunes, Y.R.F., Ochoa-gaona, S., Oliveira, R.S., Paz, H., Zimmerman, J.K., Westoby, M., 2021. Functional recovery of secondary tropical forests. Proc. Natl. Acad. Sci. 118 (49) https://doi.org/10.1073/pnas.2003405118/-/DCSupplemental.Published.
Schaap, M.G., Leij, F.J., Van Genuchten, M.T., 2001. Rosetta: a computer program for estimating soil hydraulic parameters with hierarchical pedotransfer functions. J. Hydrol. 251, 163–176. https://doi.org/10.1016/S0022-1694(01)00466-8.
Sebastian, D.E., Ganguly, S., Krishnaswamy, J., Du, K., Nemani, R., Ghosh, S., 2019. Multi-scale association between vegetation growth and climate in India : a wavelet analysis approach. Remote Sens. 11, 2073. https://doi.org/10.3390/rs11222703.
Sharma, E., Bhuchar, S., Xing, M.A., Kothyari, B.P., 2007. Land use change and its impact on hydro-ecological linkages in Himalayan watersheds. Trop. Ecol. 48, 151–161.
Siddiq, Z., Cao, K.F., 2018. Nocturnal transpiration in 18 broadleaf timber species under a tropical seasonal climate. For. Ecol. Manage. 418, 47–54. https://doi.org/10.1016/j.foreco.2017.12.043.
Singh, P., Bengtsson, L., 2005. Impact of warmer climate on melt and evaporation for the rainfed, snowfed and glacierfed basins in the Himalayan region. J. Hydrol. 300, 140–154. https://doi.org/10.1016/j.jhydrol.2004.06.005.
Singh, P., Kumar, A., 2010. Hydro-meteorological correlations and relationships for estimating stream flow for Gangotri Glacier basin in Western Himalayas. Int. J. 2, 60–69.
Sudhakar, S., Prasad, P.R.C., Arrawatia, M.L., Sudha, K., Babar, S., Rajeshwar Rao, S.K.S. V., 2008. Landscape analysis in Fambong Lho wildlife sanctuary, east district, Sikkim, India using remote sensing and GIS techniques. J. Indian Soc. Remote Sens. 36, 203–216. https://doi.org/10.1007/s12524-008-0021-3.
Tashie, A., Scaife, C.I., Band, L.E., 2019. Transpiration and subsurface controls of streamflow recession characteristics. Hydrol. Process. 33, 2561–2575. https://doi.org/10.1002/hyp.13530.
Thomas, Z., Ghazavi, R., Merot, P., Granier, A., 2012. Modelling and observation of hedgerow transpiration effect on water balance components at the hillslope scale in Brittany. Hydrol. Process. 26, 4001–4014. https://doi.org/10.1002/hyp.9198.
Tiwari, A., Khanduri, V.P., Rawat, D., Singh, B., Riyal, M.K., Mishra, G., Kumar, M., 2023. Vegetation composition, soil properties, and carbon stock of montane forests along a disturbance in the Garhwal Himalaya. India. Front. For. Glob. Chang. 6 https://doi.org/10.3389/ffgc.2023.1193792.
Ukkola, A.M., Prentice, I.C., 2013. A worldwide analysis of trends in water-balance evapotranspiration. Hydrol. Earth Syst. Sci. 17, 4177–4187. https://doi.org/10.5194/hess-17-4177-2013.
Uyup, M.K.A., Zhang, J., Feng, X., Chen, Z., Li, Z., Siam, N.A., 2023. Effect of Tree Age on the Properties of Himalayan Birch (Betula alnoides Buch.-H.ex D.Don) Wood. Bioresources 18, 8007–8019. https://doi.org/10.15376/biores.18.4.8007-8019.
van Meerveld, H.J., Jones, J.P.G., Ghimire, C.P., Zwartendijk, B.W., Lahitiana, J., Ravelona, M., Mulligan, M., 2021. Forest regeneration can positively contribute to local hydrological ecosystem services: implications for forest landscape restoration. J. Appl. Ecol. 58, 755–765. https://doi.org/10.1111/1365-2664.13836.
Vermote, E., 2015. MOD09A1 MODIS/surface reflectance 8-Day L3 Global 500m SIN Grid. NASA LP DAAC. NASA GSFC MODAPS SIPS - NASA. https://doi.org/10.5067/MODIS/MOD09A1.006.

Wang, C., Fu, B., Zhang, L., Xu, Z., 2019. Soil moisture–plant interactions: an ecohydrological review. J. Soils Sediments 19, 1–9. https://doi.org/10.1007/s11368-018-2167-0.

Wen, Z., Zheng, H., Smith, J.R., Zhao, H., Liu, L., Ouyang, Z., 2019. Functional diversity overrides community-weighted mean traits in liking land-use intensity to hydrological ecosystem services. Sci. Total Environ. 682, 583–590. https://doi.org/10.1016/j.scitotenv.2019.05.160.

Woelber, B., Maneta, M.P., Harper, J., Jencso, K.G., Payton Gardner, W., Wilcox, A.C., López-Moreno, I., 2018. The influence of diurnal snowmelt and transpiration on hillslope throughflow and stream response. Hydrol. Earth Syst. Sci. 22, 4295–4310. https://doi.org/10.5194/hess-22-4295-2018.

Wohl, E., Barros, A., Brunsell, N., Chappell, N.A., Coe, M., Giambelluca, T., Goldsmith, S., Harmon, R., Hendrickx, J.M.H., Juvik, J., Mcdonnell, J., 2012. The hydrology of the humid tropics. Nat. Publ. Gr. 2, 655–662. https://doi.org/10.1038/nclimate1556.

Wondzell, S.M., Gooseff, M.N., McGlynn, B.L., 2007. Flow velocity and the hydrologic behavior of streams during baseflow. Geophys. Res. Lett. 34, 1–5. https://doi.org/10.1029/2007GL031256.

Wright, C., Kagawa-Viviani, A., Gerlein-Safdi, C., Mosquera, G.M., Poca, M., Tseng, H., Chun, K.P., 2018. Advancing ecohydrology in the changing tropics: perspectives from early career scientists. Ecohydrology 11, 1–18. https://doi.org/10.1002/eco.1918.

Yan, C., Zhao, W., Wang, Y., Yang, Q., Zhang, Q., Qiu, G.Y., 2017. Effects of forest evapotranspiration on soil water budget and energy flux partitioning in a subalpine valley of China. Agric. For. Meteorol. 246, 207–217. https://doi.org/10.1016/j.agrformet.2017.07.002.

Yang, K.C., Hazenberg, G., 1991. Relationship between tree age and sapwood/heartwood width in Populus tremuloides Michx. Wood fiber Sci 23, 247–252.

Yang, L.Y., Yu, R., Wu, J., Zhang, Y., Kosugi, Y., Restrepo-Coupe, N., Huete, A., Zhang, J., Liu, Y.H., Zhang, X., Liu, W.J., Zhao, J.F., Zeng, J., Song, Q.H., Chen, Y.J., Song, L., Tan, Z.H., 2023. Asian tropical forests assimilating carbon under dry conditions: water stress or light benefits? J. Plant Ecol. 16, 1–23. https://doi.org/10.1093/jpe/rtac106.

Zeppel, M., Macinnis-Ng, C.M.O., Ford, C.R., Eamus, D., 2008. The response of sap flow to pulses of rain in a temperate Australian woodland. Plant Soil 305, 121–130. https://doi.org/10.1007/s11104-007-9349-7.

Zhang, R., 1997. Determination of soil sorptivity and hydraulic conductivity from the disk infiltrometer. Soil Sci. Soc. Am. J. 61, 1024–1030. https://doi.org/10.2136/sssaj1997.03615995006100040005x.